LUND UNIVERSITY

Superparamagnetic iron oxide nanoparticles (SPIONs) as a multimodality imaging probe for sentinel nodes

Design and Preclinical Evaluation

Madru, Renata

2018

Superparamagnetic Iron Oxide Nanoparticles (SPIONs) as a multimodality imaging probe for sentinel nodes

Design and Preclinical Evaluation

RENATA MADRU | DEPARTMENT OF MEDICAL RADIATION PHYSICS
FACULTY OF SCIENCE | LUND UNIVERSITY

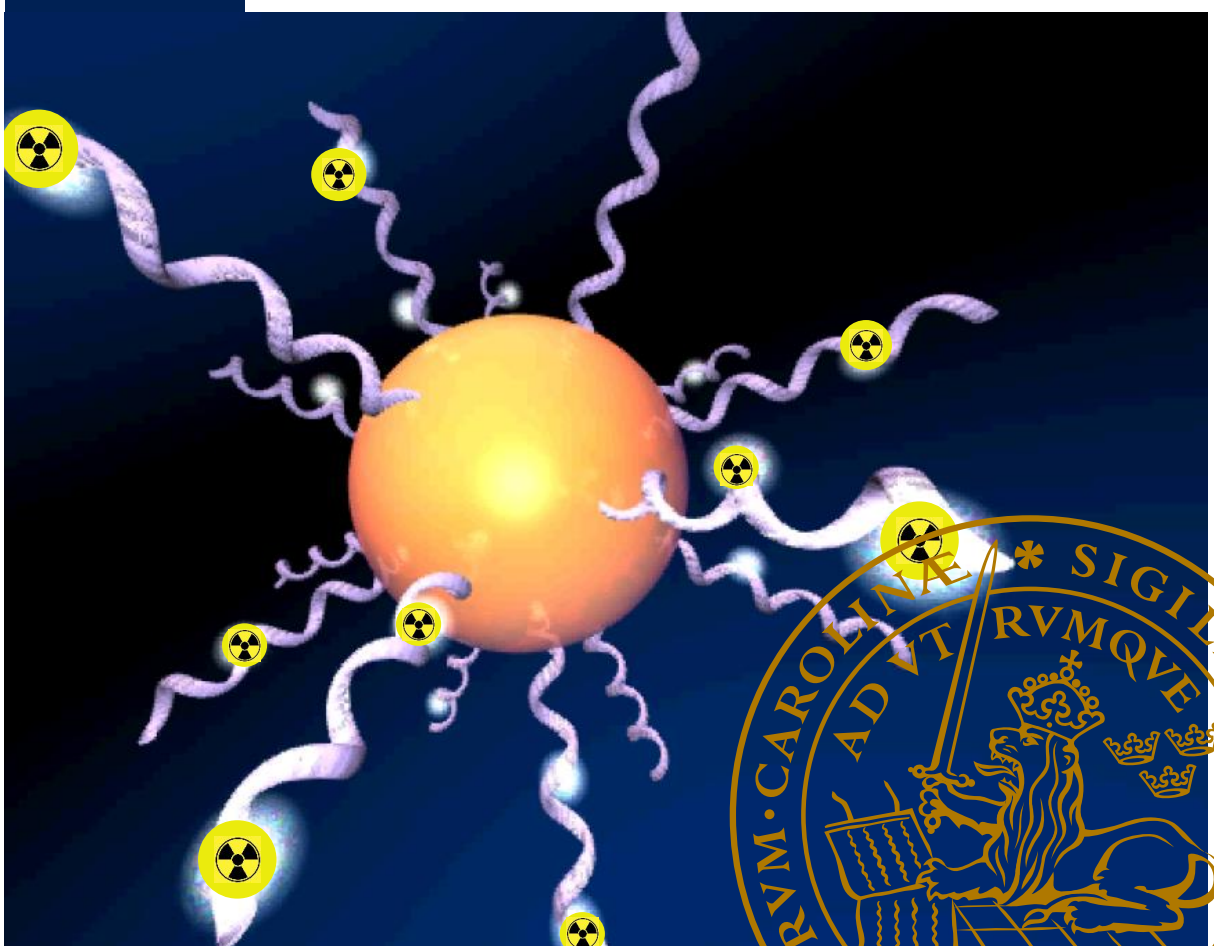

Superparamagnetic Iron Oxide Nanoparticles (SPIONs) as a multimodality imaging probe for sentinel nodes

Design and Preclinical Evaluation

Renata Madru

LUND
UNIVERSITY

DOCTORAL DISSERTATION
by due permission of the Faculty of Science, Lund University, Sweden.
To be defended at Lecture Hall F3 at Skånes University Hospital, Lund
on 17 May 2018 at 9:00.

Faculty opponent
Professor emerita Eva Lund

Organization LUND UNIVERSITY	Document name
	Date of issue
Author(s)	Sponsoring organization
Title and subtitle	

Abstract

Breast cancer and malignant melanoma disseminate through the lymphatic system and the first metastases arise in one or two regional, sentinel lymph nodes (SLNs) draining the primary tumour site. Therefore, identification and characterization of the SLNs is of major importance for cancer staging and for choice of therapy in patients. The standard clinical procedure relies on lymphoscintigraphy after intradermal injection of radiolabelled colloids (such as ^{99m}Tc-Nanocolloid in Europe) and blue dye to identify the SLNs intra-operatively. Resected SLN-biopsies are then sent for histopathological analysis. This technique, however, is limited by the non-specificity of the tracer, lack of anatomical structures as reference in scintigraphic images, and involves a tight schedule between surgery and pathological examination. In **Papers I** and **II**, we propose a new generation tracers (probes) based on superparamagnetic iron oxide nanoparticles (SPIONs) radiolabelled with ^{99m}Tc-and Cy 5.5 Alexa Fluor. SPIONs have the great advantage to be produced within a narrow size distribution (20-50 nm) optimal for transport via lymphatic vessels and accumulate in SLNs. Owing to their large surface-to-volume ratio and biocompatible coating; a high radiolabelling yield was demonstrated. After subcutaneous injection of the probe in the hind paw of Wistar rats, ^{99m}Tc-SPION-Cy 5.5 the SLNs were easily identified SPECT-MRI and optical imaging modalities. In **Paper III** and **V**, a fast one-step radiolabelling method was developed to conjugate ^{68}Ga-SPIONs and ^{64}Cu-SPIONs for positron emission tomography (PET), MRI, and Cherenkov luminescence imaging (CLI) of SLNs. After administration of the probes as in the previous papers in rats and mice, quantitative PET and MRI images were acquired simultaneously. The images clearly depicted the SLNs. A benefit of CLI is that they enable intra-operative optical imaging without the use of toxic fluorophores. In **Paper IV** non-homogeneous activity distribution in SLN was demonstrated by using digital autoradiography images (DARG), and together with data acquired from biodistribution of the agents in rats from **Paper I-III** and **V**, the absorbed doses were calculated for the different radionuclides. It has been shown that the common approach of medical intern radiation doses, MIRD, assuming a homogenous activity distribution it may underestimate the absorbed dose with a 4 fold, in some regions in SLN.

Key words		
Classification system and/or index terms (if any)		
Supplementary bibliographical information		Language
ISSN and key title		ISBN
Recipient's notes	Number of pages	Price
	Security classification	

Signature  Date 2018/04/18

Superparamagnetic Iron Oxide Nanoparticles (SPIONs) as a multimodality imaging probe for sentinel nodes

Design and Preclinical Evaluation

Renata Madru

LUND
UNIVERSITY

Department of Medical Radiation Physics,
Lund University Sweden

Coverphoto by Olof Strandberg

Faculty of Science, Lund University
Department of Medical Radiation Physics

ISBN 978-91-7753-685-7
ISSN 978-91-7753-686-4

Printed in Sweden by Media-Tryck, Lund University
Lund 2018

List of contents

Abstract

Breast cancer and malignant melanoma disseminate through the lymphatic system and the first metastases arise in one or two regional, sentinel lymph nodes (SLNs) draining the primary tumour site. Therefore, identification and characterization of the SLNs is of major importance for cancer staging and for choice of therapy in patients. The standard clinical procedure relies on lymphoscintigraphy after intradermal injection of radiolabelled colloids (such as ^{99m}Tc-Nanocolloid in Europe) and blue dye to identify the SLNs intra-operatively. Resected SLN-biopsies are then sent for histopathological analysis. This technique, however, is limited by the non-specificity of the tracer, lack of anatomical structures as reference in scintigraphic images, and involves a tight schedule between surgery and pathological examination. In **Papers I** and **II**, we propose a new generation tracers (probes) based on superparamagnetic iron oxide nanoparticles (SPIONs) radiolabelled with ^{99m}Tc-and Cy 5.5 Alexa Fluor. SPIONs have the great advantage to be produced within a narrow size distribution (20-50 nm) optimal for transport via lymphatic vessels and accumulation in SLNs. Owing to their large surface-to-volume ratio and biocompatible coating, a high radiolabelling yield was demonstrated. After subcutaneous injection of the probe in the hind paw of Wistar rats, ^{99m}Tc-SPION-Cy 5.5 the SLNs were easily identified using SPECT-MRI and optical imaging modalities. In **Paper III** and **V**, a fast one-step radiolabelling method was developed to conjugate ^{68}Ga-SPIONs and ^{64}Cu-SPIONs for positron emission tomography (PET), MRI, and Cherenkov luminescence imaging (CLI) of SLNs. After administration of the probes as in the previous papers in rats and mice, quantitative PET and MRI images were acquired simultaneously. The images clearly depicted the SLNs. A benefit of CLI is that they enable intra-operative optical imaging without the use of toxic fluorophores. In **Paper IV** non-homogeneous activity distribution in SLN was assumed. By using digital autoradiography images (DARG) and data from biodistributions of the agents injected in rats (data from **Paper I-III** and **V)**, the absorbed doses were calculated for the different radionuclides. It has been shown that the common approach of medical intern radiation doses, MIRD, assuming a homogeneous activity distribution it underestimates the absorbed dose in some regions in SLN.

Populärvetenskaplig sammanfattning

Bröst- och hudcancerceller sprider sig via lymfatiska systemet och förankrar sig i en eller två regionala sentinel lymfnoder (SLN) där de med stor sannolikhet växer till metastaser. Därför är SLN-biopsier och relaterade histopatologiska undersökningar viktiga vid cancerdiagnostiken för att bestämma sjukdomsstatus och att från denna kunna bestämma rätt behandling. Patienter vars lymfnoder innehåller spridda cancerceller har nämligen ofta en sämre prognos.

För gällande kliniska rutinproceduren injiceras radioaktivt märkta små partiklar (sk kolloider) direkt under huden på patienten och i nära anslutning till tumörområdet. Efter några timmar har en del av kolloiderna ansamlats i SLN och kan där avbildas med en gammakamera för att identifiera läget på lymfkörteln, som skall avlägsnas för biopsi. Dessa bilder visar dock bara upptag och innehåller ingen anatomisk vägledning som kirurgen kan orientera sig efter. Därför injiceras även ett blått spårämne som färgar lymfnoderna och även lymfvägen ifrån tumörområdet, exempelvis mot armhålan. Därefter mäts mängden radioaktivitet i de blåa noderna med hjälp av en handhållen detektor. Den nod med högst mätvärde antas då vara SLN. Denna skärs då bort och undersöks, med avseende på närvaro av cancerceller, genom mikroskopi under tiden som själva primärtumören tas bort. Hela proceduren verkar vara ganska enkelt men har flera steg att ta hänsyn till, nämligen a) att man använder flera spårämnen varav ingen av dem är speciellt specifik, b) man utsätter personal för en liten men dock en stråldos och c) proceduren kräver en djup erfarenhet av kirurgen.

Målet med delprojekten i avhandlingen var därför att utveckla ett bättre spårämne, som är baserat på järnoxid-nanopartiklar, s.k. SPIONs och som storleksmässigt är optimala för att snabbt transporteras från injektionsstället via lymfan till SLN. Detta spårämne kan sedan avbildas med, exempelvis, en magnetresonanskamera (MRI). Trots fördelarna med en hög upplösningen och frånvaron av joniserande strålning har MR-kameran en dålig känslighet jämfört med de nuklearmedicinska bildgivande systemen SPECT och PET. Därför märktes SPIONs också kemiskt med radionukliden ^{99m}Tc. I **Arbete I** beskrivs här en effektiv inmärkningsprocess av ^{99m}Tc med högt utbyte. Efter att ha injicerat i huden på bakbenen hos råttor kunde SLN avbildas med både MR och SPECT system. Dessutom kunde ^{99m}Tc-SPIONs också detekteras med den handhållna detektorn under själva biopsitagningen. ^{99m}Tc-SPIONs biokinetik i råttor studerades också och med avseende på i vilka andra organ spårämnes ansamlades. Djurstudier är i allmänhet ett viktigt steg för att kunna uppskatta strålningsrelaterade effekter och andra toxiska risker innan ämnet kan användas på patienter.

I **Arbete II**, kopplade vi fluorophor-molekyler (Cy 5.5, Alexa Fluor) till de radioaktivt-märkta ^{99m}Tc-SPIONs. Målet var att ersätta de två olika spårämnena (^{99m}Tc-kolloider och det blå färgämnet) med en enda ”probe” som kan avbildas med både SPECT och MR och även med en sk ”bed-side” optisk kamera som kan ”lysa upp” SLN:na under biopsin. I detta arbete har även utförts en biokinetiksstudie av ^{99m}Tc-SPIONs-Alexa Fluor. I samband med dessa studier har SLN:er innehållande radioaktivitet frysts, snittats och monterats på mikroskopiglas för att undersökas med digital autoradiografi (DARG) och fluorescens-mikroskopi. Aktivitetsfördelningen överensstämde väl med mikroskopibilderna. Partiklarna förekom som förväntat mest extracellulärt, i de subkapsulära sinusarna och i hilum i SNL.

De senaste åren har utvecklingen inom onkologi skett snabbt och SPECT/CT kameror har kompletterats med PET/CT system som med modern teknik ger bilder med bättre rumsupplösning.

För att kunna utföra kvantitativa, dynamiska biokinetik studier, har vi i **Arbete III och V**, utvecklat en ^{68}Ga-SPION variant med halveringstiden 68 min och en ^{64}Cu-SPION med en längre halveringstid av 12.7 h för att användas på PET/MR system. Vi har också, i detta arbete, visat att ^{68}Ga-SPIONs även kan användas vid Cherenkov Luminescense Imaging (CLS). Detta är en typ av optisk bildtagning som kan lämpa sig för biopsier, liknande sätt som med hjälp av fluorophor. Fördelen med fluorophoren är dess längre våglängd jämfört med den blå våglängd som används vid CLS. Däremot vid ^{68}Ga-fallet, själva radionukliden som emitterar ljuset (när elektronerna bromsas upp i vävnaden och genom växelverkan avger sin energi). Detta medför att tiden för inmärkning för ^{68}Ga-SPIONs kan halveras, och injektion av eventuella toxiska fluorophorer kan undvikas. Både metoderna använder samma typ av CCD kamera för själva optiska bildgivningen.

Arbete IV fokuseras mot dosimetri för dessa undersökningar. Målet med detta arbete var att jämföra aktivitetsfördelningen i patienters SLN med den fördelning i SNL man kan se i djur SLN och vi har studerat dessa fördelningar för olika radionuklider och deras dosimetriska egenskaper. Istället för att använda organ-baserat dosberäkningar har vi utgått ifrån DARG-bilderna där vi segmenterar olika volymer, baserat på skillnader i aktivitetskoncentrationer. Resultaten visar att den absorberade dosfördelningen också är heterogen inom SLN, och den absorberade dosen kan vara upp till 4 ggr högre i vissa delar av SNL jämför med om man hade räknat med jämt radioaktivitetsfördelning.

Abbreviations

CT	Computed Tomography
CLS	Cherenkov Luminescence Imaging
DARG	Digital Autoradiography
DLS	Dynamic Light Scattering
EMA	European Medicine Agency
EPR	Enhanced Permeability and Retention
FDA	Food and Drug Administration
FDG	Fluorodeoxyglucose
IA	Injected Activity
ID	Injected Dose
MRI	Magnetic Resonance Imaging
NIR	Near Infrared
OI	Optical Imaging
PET	Positron Emission Tomography
PEG	Polyethylene Glycol
p.i.	post injection
RES	Reticuloendothelial System
s.c.	subcutaneous
SLN	Sentinel Lymph Node
SPECT	Single Photon Emission Computed Tomography
SPION	Superparamagnetic Iron Oxide Nanoparticle
TEM	Transmission Electron Microscopy
USPIO	Ultrasmall Superparamagnetic Iron Oxide Nanoparticle

List of original papers

I. **^{99m}Tc-labeled superparamagnetic iron oxide nanoparticles for multimodality SPECT/MRI of sentinel lymph nodes.**
Renata Madru, Pontus Kjellman, Fredrik Olsson, Karin Wingårdh, Christian Ingvar, Freddy Ståhlberg, Johan Olsrud, Jimmy Lätt, Sarah Fredriksson, Linda Knutsson, Sven-Erik Strand.
Journal of Nuclear Medicine, 2012, 53:459-463.

II. **Development of a Hybrid Nanoprobe for Triple-Modality MR/SPECT/Optical Fluorescence Imaging.**
Renata Madru, Pontus Svenmarker, Christian Ingvar, Freddy Ståhlberg, Stefan-Andersson Engels, Linda Knutsson, Sven-Erik Strand.
Diagnostics, 2014, 10; 4(1):13-26.

III. **^{68}Ga-labeled superparamagnetic iron oxide nanoparticles (SPIONs) for multi- modality PET/MR/Cherenkov luminescence imaging of sentinel lymph nodes.**
Renata Madru, Thuy A. Tran, Johan Axelsson, Christian Ingvar, Adnan Bibic, Freddy Ståhlberg, Linda Knutsson, Sven-Erik Strand.
American Journal of Nuclear Medicine and Molecular Imaging, *2013*, *4:6069.*

IV. **Absorbed dose and dose distribution of radiolabelled superparamagnetic iron oxide nanoparticles (SPIONs) in sentinel lymph nodes.**
Renata Madru, Erik Larsson, Anders Örbom, Christian Ingvar, Dorthe Grabau, Sven-Erik Strand.
To be submitted to JNM

V. **Simultaneous preclinical PET/MRI study of lymphatic drainage of ^{64}Cu-SPIONs.**
Renata Madru, Michael Budassi, Hedok Lee, David S. Smith, Paul Vaska, Linda Knutsson, Sven-Erik Strand.
Cancer Biotherapy and Radiopharmaceuticals-Accepted April 2018

Thesis at glance

Paper I

Purpose: To develop and characterize the radiolabelled superparamagnetic iron oxide nanoparticles *in vitro* and *in vivo* and to evaluate the feasibility of the agent to detect sentinel lymph nodes (SLNs) in rodents.

Methods: SPIONs were labelled with ^{99m}Tc. The labeling efficiency and stability were evaluated in buffer solution and human serum. A pilot animal study was performed using clinical SPECT and MRI systems to evaluate ^{99m}Tc-SPIONs stability *in vivo*.

Conclusion: ^{99m}Tc-SPIONs were demonstrated to be stable *in vitro* and *in vivo*. The SLNs were clearly visualized with both SPECT and MRI clinical imaging systems.

Paper II

Purpose: To label SPIONs with ^{99m}Tc and a fluorophore for triple SPECT-Optical-MRI imaging and test its feasibility to image SLNs using three different imaging modalities.

Methods: SPIONs were labelled with ^{99m}Tc and Cy 5.5 Alexa Fluor. White Wistar rats were injected with the agent in the right hind paw and imaged with SPECT, a CCD-based optical imaging instrument and MRI to detect the SLNs. Histology studies were performed to localize the uptake within the SLNs.

Conclusion: The SLNs were visualized with all three imaging modalities. The ^{99m}Tc - Cy 5.5 Alexa –SPIONs were found to accumulate in the subcapsular sinuses and in medullary sinuses in healthy SLNs.

Paper III

Purpose: To label the SPIONs with ^{68}Ga for simultaneous PET-MRI and intraoperative Cherenkov imaging. ^{68}Ga became available as generator-produced radionuclide with good potential for nuclear medicine imaging.

Methods: A direct labelling method was developed, and the stability of the ^{68}Ga-SPIONs was evaluated in serum and in vivo. Wistar rats injected subcutaneously in the hind paw were imaged with PET, MRI and a slow-scan deep-cooled CCD camera for Cherenkov luminescence imaging.

Conclusion: A labelling efficiency over 95 % was reached in 10 min. The ^{68}Ga-SPIONs enabled visualization of SLNs via all three imaging modalities. Cherenkov imaging was demonstrated to be a very efficient method to visualize superficial lymph nodes with potential for translation to the clinic.

Paper IV

Purpose: First, to compare the distribution of the ^{99m}Tc-nanocoll in human SLNs with the ^{99m}Tc-SPIONs and ^{68}Ga-SPIONs distributions in rat lymph nodes using high resolution digital autoradiography. Second, based on digital autoradiography imaging, to calculate the absorbed dose and the absorbed dose distribution in SLNs and risk organs.

Methods: Frozen section of harvested lymph nodes from breast cancer patients injected with ^{99m}Tc-Nanocoll, and rats injected with ^{99m}Tc- and ^{68}Ga-labelled SPIONs were imaged using digital autoradiography. Then the absorbed dose rates and the absorbed dose for different regions within the SLNs were calculated.

Conclusion: Digital autoradiography images revealed a heterogeneous activity distribution of ^{99m}Tc-Nanocoll, ^{99m}Tc-SPIONs and ^{68}Ga-SPIONs within the SLNs. Consequently, a non-uniform activity- and absorbed dose distribution was shown, it's pattern depending on the geometry and radiation emission energy spectrum. As a result, the absorbed dose to structures within some regions was 2-3 folds higher when using small-scale dosimetry model and compared to the mean absorbed dose to the whole organ.

Paper V

Purpose: To label the SPIONs with ^{64}Cu for simultaneous PET-MRI imaging and follow the biodistribution of the tracer up to 24 h.

Methods: Direct labelling method was used for conjugation. Mice were injected with ^{64}Cu-SPIONs in the hind paw and imaged with 9.4T MRI using an integrated PET scanner.

Conclusion: The use of a single hybrid probe and simultaneous hybrid imaging provides an efficient, complementary integration of quantitation and is expected to improve pre-operative planning and intra-operative guidance for cancer treatments.

List of contributions

Paper I

We planned the study together with the other authors. I was responsible for execution of this study. I developed the radiolabeling protocols, conducted the in vitro and in vivo studies. Karin Wingårdh assisted with the animal experiments while Johan Olsrud and Jimmy Lätt assisted with the MRI imaging. I was responsible to analyse the results and I was the main author of the manuscript.

Paper II

I planned and executed the study. I developed the radiolabelling protocols, quality control, conducting animal studies, and analysing the data. The optical imaging part was conducted in collaboration with Pontus Svenmarker and Stefan-Andersson Engels. I was the main author of the manuscript.

Paper III

I have been involved in the majority of this work. The radiolabeling protocol was developed with help from Thuy Tran. I was responsible for conducting the animal studies (PET/CT) and biodistribution. With the MRI imaging I was assisted by Adnan Bibic and the Cherenkov imaging part was conducted in collaboration with Johan Axelsson. I was the main author of the manuscript.

Paper IV

We planned the study together with the other authors. I collected the patient data and conducted the animal studies. I was responsible for a part of the data analysis while the dosimetry calculations were conducted by Eric Larsson. I was the main author of the manuscript.

Paper V

I planned the study, developed the radiolabelling protocol and analysed the data. The execution was performed in collaboration with the other authors. I was the main author of the manuscript.

1. Introduction

Cancer is an increasing health issue worldwide due to prolonged life spans, social norms and environmental influences. The most common cancer types in Sweden are prostate cancer, breast cancer and cutaneous malignant melanoma.[1] The success rate in curing these cancer types is high when diagnosis is performed at an early stage and if the correct treatment method is provided. Therefore it is essential to stage the cancer, which is to determine the primary tumour size, characterize the cancer cells using biopsies and to determine if they have spread in the body.

Breast cancer and malignant melanoma mainly disseminate through the lymphatic system and the first metastases most often arise in the sentinel lymph nodes (SLNs), defined as the first nodes draining the primary tumour site.[2] Therefore, the pathological status of the SLNs determines both prognosis and choice of therapy.[3] At present, accurate identification and in vivo characterization of SLNs is, however, still challenging.

The current gold standard for identifying SLN's is based on pre-operative lymphoscintigraphy after interstitial, periareolar injection of radiolabelled colloids, 2-24 h prior to surgery. In addition, a blue dye is injected close to the primary tumour site in order to highlight the draining lymphatic vessels and SLNs during intraoperative biopsy sampling.[4] The SLNs are then identified both due to blue staining and the activity content measured using a hand-held gamma-probe (Fig. 1). The resected 1-3 SLNs are then sent for histopathological examination. Metastatic cells present in the SLN biopsies implies worse prognosis for the patient and a more advanced treatment in addition to surgery or external radiation therapy.

Although relatively high SLN identification rates (85-98 %) are reported in axilla, collateral lymph flow may occur in both breast cancer and malignant melanoma patients leading to false-negative results as high as 5-10 % and 53 % respectively.[5-7] Because scintigraphy images lack morphological information, pre-operative planning and identification of SLNs may rely on the experience of the surgeon. In prostate-, head and neck, gastro, urological and gynaecological cancers this method is still under evaluation mainly because of the non-specificity of the tracers.

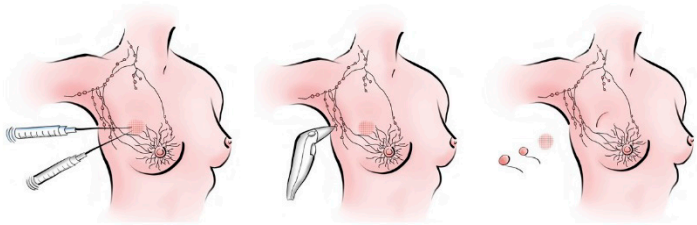

Fig. 1
Current technique for SLN biopsy. Left: administration of radiolabelled colloids. Middle: detection of SLNs with hand-held gamma probe. Right: dissection of the SLN.

Development of robust imaging techniques in combination with specifically designed contrast agents may improve nodal assessment before surgery (Paper I-III). Conventional cross-section imaging modalities such as ultrasonography, computed tomography (CT) and magnetic resonance imaging (MRI) providing morphological information have relatively low accuracy in predicting the SLN status.[8-10] However, by combining high-resolution MRI with high-sensitivity SPECT, PET or optical imaging modalities, using multimodal contrast agents, more accurate and less invasive identification of SLNs is possible (Paper III and V).

New generation contrast agents, smartly designed liposomes, dendrimers, quantum dots and magnetic nanoparticles provide many advantages in comparison with traditional radiolabelled colloids. These include fast clearance from the injection site, increased uptake and sustained retention in SLNs, detection using different imaging modalities simultaneously or carrying drugs for therapy.[11-14]

Superparamagnetic iron oxide nanoparticles (SPIONs) have gained much attention due to their low toxicity and intrinsic paramagnetic properties when an external magnetic field is applied. Following intravenous or subcutaneous administration, SPIONs are transported via lymphatic vessels into the SLNs where they provide a negative contrast in MRI using T2 and T2*-weighted imaging protocols. Diseased lymph nodes present a non-homogenous uptake of SPIONs which may help to differentiate between metastatic and healthy lymph nodes in vivo.[15-16] Because SLNs with black staining provides a low contrast in MRI, it could be difficult to distinguish them from other structures i.e. blood vessels. Therefore, it is advantageous if this technique can be combined with other imaging modalities such as quantitative, high sensitivity PET by radiolabelling the SPIONs with radionuclides.

What is proposed in this thesis is to develop a new contrast agent for a more accurate identification and characterization of SLNs using SPIONs and multimodal imaging. The SPIONs consist of a solid iron oxide core, coated with

polyethylene glycol (PEG) to avoid aggregation and to enable further functionalization. The size of the SPIONs will be optimized for fast clearance from the injection site and high uptake in SLNs. Detection of SLNs will be evaluated with different imaging modalities including radionuclide-based SPECT/PET and optical imaging modalities. Biodistribution and dosimetric calculations have been conducted for comparison with traditional tracers, in the hope of future clinical translation.

2. Aims

The overall aim of these studies was to develop a new imaging agent based on superparamagnetic iron oxide nanoparticles (SPIONs). The SPIONs need to fulfil particular criteria for size, *in vivo* colloidal stability, biocompatibility, and it should be possible to detect them simultaneously with different imaging modalities. MRI-PET is an emerging powerful tool with potential for in vivo characterization of SLNs. Currently, there is no dual- tracer/probe commercially available for SLN imaging. In addition, optical imaging using fluorophores (with emission in the near infra-red, NIR), and Cherenkov Luminescence imaging have been investigated for surgical guidance and resection of SLNs.

The overall goals were:

- To characterize SPIONs (shape, size, surface charge) and label them with ^{99m}Tc for in vivo detection of SLNs in rodents. To study the distribution of ^{99m}Tc-SPIONs in SLNs using DARG imaging (Paper I).
- To label the SPIONs with ^{99m}Tc and fluorophores for tri-modal MR-SPECT-Optical imaging of SLNs and study the stability and biodistribution of these nanoprobes in rodents. (Paper II)
- To label the SPIONs with ^{68}Ga for simultaneous MRI-PET and intraoperative Cherenkov imaging. (Paper III)
- To calculate the absorbed dose based on digital autoradiography images of SLNs from patients and compare with absorbed doses resulting from the animal studies. (Paper IV)
- Simultaneous MRI-PET imaging to monitor animals injected with radiolabelled ^{64}Cu-SPIONs over a period of several days in order to determine the accumulation, retention and clearance of the agent in SLNs was carried out. (Paper V)

3. Concept image

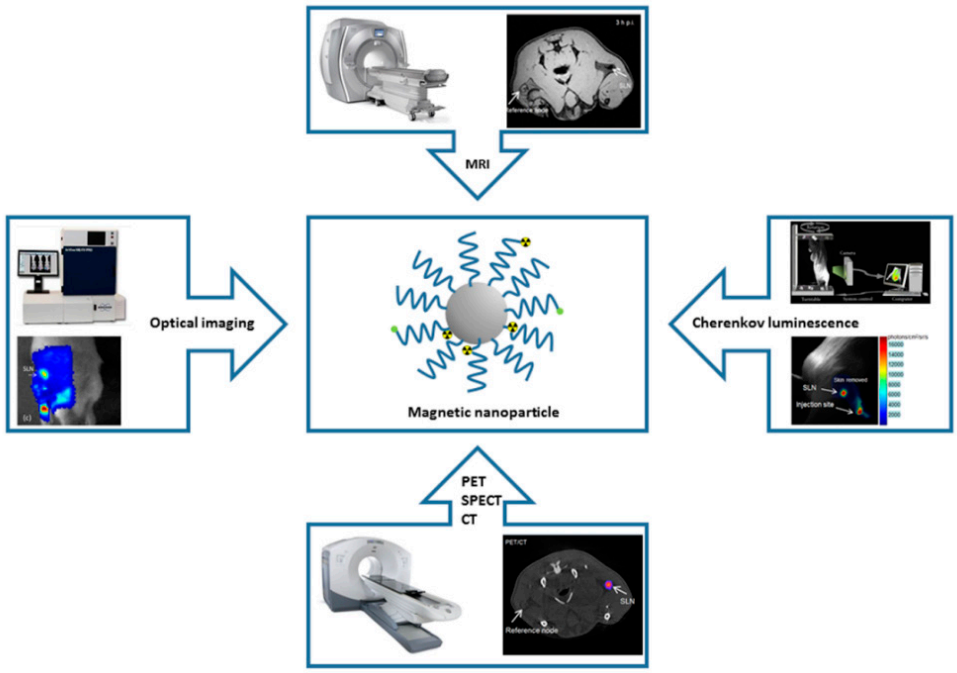

Fig. 2
Development of a hybrid probe to target organs of interest and visualize it with different imaging modalities.

Table 1
Contrast agents developed for simultaneous, multimodal imaging.

	Paper	MRI	SPECT	PET	Optical – NIR	Optical – CLI
99mTc-SPIONs	I	x	x			
99mTc-SPIONs-AF	II	x	x		x	
68Ga-SPIONs	III	x		x		x
64Cu-SPIONs	IV	x		x		

4. Background

To develop an optimal probe for SLN imaging requires understanding of the function and morphology of the lymphatic system. A brief summary of the mechanism that mediates the uptake and retention of radiolabelled nanoparticles in lymph node structures is here presented. However, physiological aspects i.e. lymph formation and structures of other lymphoid tissues like thymus, spleen and bone marrow will not be covered.

The lymphatic system

The lymphatic system is a part of the circulatory system, consisting of a network of capillary and collecting vessels, lymph (similar to blood plasma) and lymphoid tissue such as lymph nodes, bone marrow, spleen and thymus. Unlike the cardiovascular system, the lymphatic system is unidirectional and its main function is to collect interstitial fluid from the extracellular space in tissue, as well as macromolecules, and proteins, and return them into the bloodstream through one of the subclavian veins.[17] Apart from maintaining fluid balance in the body and homeostasis, the lymphatic system removes cellular debris and foreign bodies and has a key role in mediating immune response; it is a route for immune cells such as lymphocytes, macrophages, and host B- and T-cells.[18]

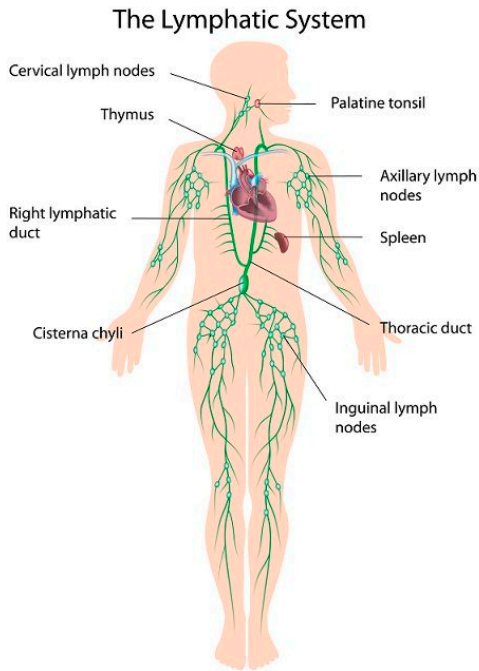

Fig. 3
The lymphatic circulatory system, including organs and vessels.

Lymphatic vessels

The removal of macromolecules, particles and waste products takes place at the interface between capillaries and tissue (Fig 4). The capillaries are lined with thin-walled endothelial cells fixed to the surrounding extracellular matrix by anchoring filaments of elastic fibres.[19] The inner endothelial cell layer also contains junctions (up to 200 nm in diameter) that are normally closed but open when the interstitial pressure increases. The junctions have small valves that block backflow.

Capillaries lack muscle cells and the lymphatic system does not have a pump. The lymph is pushed forward by the blood circulatory system into larger, impermeable collecting vessels with fully formed basement membranes encasing a hybrid between smooth and cardiac muscle cells able to contract and relax for propulsion of lymph.[20] Respiratory movements and muscular activity including massage increase the lymph flow. Whereas, resting or use of anaesthesia slows down the lymph propulsion, and this depression can vary considerably with the anaesthetic used.[21]

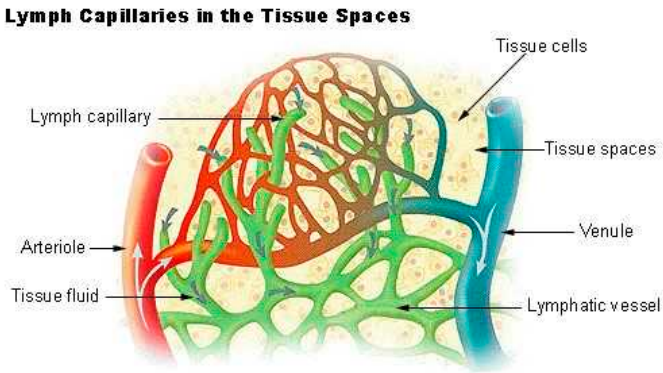

Fig. 4
Interface between lymphatic capillaries, tissue and the cardiovascular system. Fluid from interstitial space is absorbed within the lymphatic system, are transported and "filtered" in lymph nodes and then transported back into the bloodstream.

Lymph nodes

The lymph nodes are distributed in clusters along the lymphatic network and receive lymph through several afferent vessels. The lymph from each afferent vessel enters via subcapsular sinuses in a compartment (lobule) containing the deep cortex and medullary sinuses. The sinuses are traversed by a fine reticular meshwork composed of elongated fibroblastic reticular cells where particles can be mechanically trapped or phagocytized by macrophages lining up by the sinus walls. The lymph leaves the nodes via the efferent lymphatic vessel at the hilus.[22] Because there are fewer efferent vessels than afferent vessels the outflow is slow.

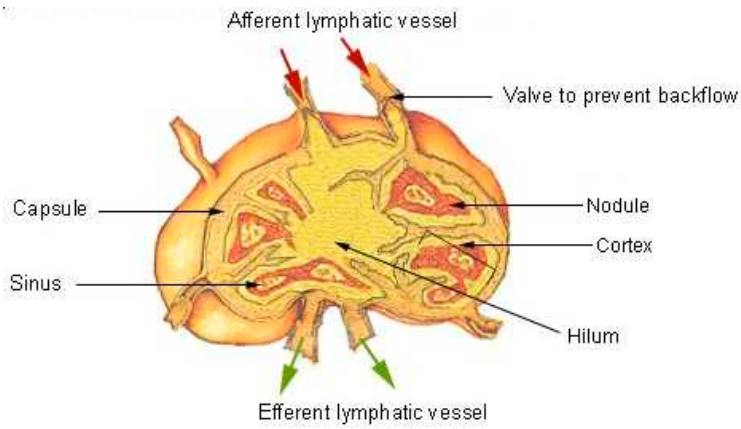

Fig. 5
The inner structures of a lymph node including the hilum, nodules, cortex and capsule are presented in this figure.

Transport of metastatic cells

The lymphatic system is used by metastatic cells to disseminate. The free tumour cells are absorbed in the capillaries and transported with the lymph into the SLNs. Studies have also shown that as a response to active signalling of tumour cells; capillary vessels are able to invade tumours and induce lymph angiogenesis.[23-25] Therefore, the lymphatic system is equally important as the vascular system as a route for targeted therapy and diagnosis of cancer.

Nanoparticles

First generation radiolabelled colloids for SLN detection

Radiolabelled colloids such as thorium dioxide, colloidal carbon and gold (^{198}Au) were developed and used for clinical examination of the reticulo-endothelial system (RES), liver and bone marrow using scintigraphy as early as the late 1940s. Lymphatic drainage was first studied in pelvic cancer patients using interstitially injected ^{198}Au colloids in late 1950s.[26] Colloids were adsorbed into the lymphatic vessels and accumulated in regional, healthy and metastatic lymph nodes.[27] Autoradiography images showed that the colloids are more likely to accumulate in the residual normal tissue of cancer-invaded lymph nodes.[28]

Since the 1950's, a large number of ^{99m}Tc-labelled colloids have been developed (Table 2). Lymphoscintigraphy has been established as an important tool in staging breast cancer and malignant melanoma. Based on their preparation techniques, these colloids vary widely in size and pharmacokinetic properties.[29]

Table 2
Radiopharmaceuticals for detection of SLNs (table adapted guidelines in Pasqualini, Bergqvist et al., and Buscombe et al) .

Radiopharmaceuticals	Size distribution (nm)	Approved
^{99m}Tc-HSA	< 80	Europe
^{99m}Tc-sulphur colloid	5-5000	USA
^{99m}Tc-Nanocolloid	5-100	Europe
^{99m}Tc- stannous hydroxide	30 – 200	Europa
^{99m}Tc- antimony trisulphide	3-30	Canada, Australia
^{99m}Tc-Rhenium sulphide	8 – 68	Europe
^{99m}Tc- dextran (Lymphoseek)		Europe

Strand et al reported that tracers should have a colloid size of less than 100 nm for a relatively fast clearance from the injection site and accumulation in the SLNs.[29] ^{99m}Tc-sulfur colloids, the commonly used tracer for SLN imaging in USA, were reported to have an average colloid size of 305- 340 nm, and by filtration the size range can be limited to colloids of smaller than 200 nm.[30] ^{99m}Tc-Nanocoll and ^{99m}Tc-human serum albumin (HSA) used in Europe, typically consist of colloids smaller than 80 nm. Still, the uptake of the tracer in SLNs after subcutaneous or interstitial injection is in range of only 1-3 % of the injected activity, as measured 2-12 h post-injection.[31] Therefore, there is a need for the development of new tracers that meet the size criterion for the optimal imaging agent, undergo fast clearance from the injection site, and have good retention in the SLNs.

^{99m}Tc-Tillmanocept was recently approved for clinical use in Europe. The tracer consists of a dextran backbone, conjugated with mannose receptors that target lymph node macrophages for an increased uptake and retention in SLNs of breast cancer patients.[32] Receptor mediated uptake was also reported by Li et al. targeting the CD20 antigen which is expressed on the surface of B-cells in SLNs.[33] This tracer has shown a high sensitivity and specificity, identifying SLNs with 98.8 % accuracy in a study conducted on 2317 breast cancer patients.

Second generation, nanoparticle-based contrast agents for SLN detection

“Nanoparticles are small colloidal particles, but not all small colloidal particles are nanoparticles.” – Johannes Lyklema, Wageningen University & Research, Wageningen, Netherlands.

Nanoparticles are structures smartly designed with unique properties in the size range of 1-100 nm, demonstrating high potential for in vivo molecular imaging

and cancer diagnosis. The nanoparticles core can be synthetized from natural proteins, polymers, dendrimers, lipid-water micelles, metal oxides or ceramics. For in vivo applications, nanoparticles are generally coated with biocompatible hydrophilic polymers or polyethylene glycol (PEG) in order to reduce their uptake by the reticuloendothelial (RES system). The large surface to volume ratio allows functionalization with multiple bioadhesive sites for radionuclides and other contrast agents for multi-modality imaging. The signal is generated by the nanoparticles core, as in the case of superparamagnetic iron oxide nanoparticles (SPIONs) or other molecules incorporated in the formulation, such as gadolinium, quantum dots, fluorophores and radionuclides using an appropriate imaging modality.[11, 34-35]

SPIONs are produced either through high temperature hydrophobic crystal growth or precipitation of alkaline solutions containing iron salts (Fe^{2+}, Fe^{3+}) and coated with biocompatible dextran or polymers to prevent aggregation.[36-37] Iron is considered to enter into the normal iron metabolism after phagocytization of the SPION by the RES. Several SPION formulations have already been FDA approved for human use such as Feridex® and Resovist® for detection of liver metastasis, Combidex® (ferumoxtran-10) for SLN detection in patients with prostate cancer and Ferohem® (ferumoxytol) to treat iron deficiencies. SentiMag® (based on carbodextran coated SPIONs, Sienna®) is under clinical trial for SLN identification.

The nanoparticles suitable for SLN imaging need to fulfil several basic criteria such as: biocompatibility, optimal size, charge, colloidal stability, strong contrast at low doses, bioconjugation and targeting ability. These criteria serve as the basis for selecting ultrasmall-SPIONs (or USPIONs) for SLN imaging.

Characterization of the nanoparticles

Depending on the size range and composition of the nanoparticles there are several techniques available to measure them. A full characterization of the nanoparticles may require more than one technique. The most common characteristics are size, shape, charge and molecular stability in bulk solutions.

Size and shape

The size of the nanoparticles can be measured by several techniques; the most common ones are listed in **Table 3**.

Transmission electron microscopy (TEM) can image and measure the size of nanoparticles at a spatial resolution down to 1 nm. A thin (< 100 nm) sample supported on a carbon or copper grid must be prepared and dried. Then, high energy electron beams are used to interact with the sample in a vacuum chamber. The scattered and unscattered electrons are focused by a series of lenses and projected onto a screen to generate an image of the nanoparticles.[39] Dehydration and the heat from the electron beam may affect the coating of the nanoparticles and the resulting size measurements.

Scanning electron microscopy (SEM) is another technique that uses high energy electron beams to scan the sample and render detailed images of the surface of the nanoparticles.[40] The size, size distribution and the shape of the nanoparticles can be determined. The sample is usually spread on a polycarbonate filter, dried and coated with a thin electrically conducting material by sputtering.[41] Sample preparation can be time consuming and the drying process may cause shrinkage of the coating. This technique is usually applied as a complement to TEM to image the surface (shape) of the nanoparticles.

Dynamic light scattering (DLS) can measure nanoparticle size distributions from submicron down to one nanometer, in solutions using monochromatic light e.g. lasers.[42] The technique relies on monitoring the temporal fluctuations of the elastic scattering of the light, induced by the Brownian motion of the nanoparticles in the solution. The size of the nanoparticles is derived using the motion-dependent autocorrelation function based on the Stokes-Einstein equation. This technique is less invasive in comparison with the techniques mentioned above; the sample preparation is less complicated and less time consuming. However, the sensitivity of this technique decrease for small particles; impurities like dust or aggregated nanoparticles can interfere and affect the results of the measurements.[39]

X-ray diffraction (XRD) is used mainly for crystalline or polycrystalline materials, to study individual crystals at the atomic scale. However, this technique can be time consuming, requires a large volume of sample and low intensity of the diffracted X-rays in comparison with electron diffractions methods.

Table 3.
Common techniques for size measurements and characterization of the nanoparticles.

Technique	Measures	Sample	Sensitivity	Notes
Transmission Electron Microscopy (TEM)	particle size and shape	-spotted on a copper grid and dried	1 nm	- sample preparation is time consuming - it may underestimate the size of the NP + images of the NP are obtained
Scanning Electron Microscopy (SEM)	particle size and shape	-dried and coated e.g. gold-palladium alloy	1 nm	- freeze-fraction technique recommended - it may underestimate the size of the NP + images of the NP are obtained
Dynamic Light Scattering (DLS)	average particle size and size distribution	- dispersed in liquid phase -concentrations 1-10 mg/mL	1 nm	- it may overestimate the size of the NP - the concentration and type of ions in the medium may affect the measurements + fast method
X-Ray Diffraction (XRD)	average particle size in a bulk sample	- crystalline materials -large samples are required (> 1 mg)	1 nm	- less available + can identify individual crystals

Charge

Zeta-potential measurements characterize the surface-liquid interfaces of SPIONs. This potential is defined as the electrical potential at the slipping plane. The iron oxide core has a tendency to build up a surface charge in solutions and attract ions of opposite charge in the vicinity. This will result in a double layer surrounding the nanoparticles one layer of firmly bond ions of opposite charge and another diffuse layer of loosely associated ions. The thickness of this double layer is dependent on the strength of the ionic solution.[43] The slipping plane is considered to be thinner than the double layer but there is no consensus or clear definition for it in the literature. The zeta potential or shift of slipping plane may be calculated by measuring the streaming current potential or electrophoretic mobility.[44-45]

The zeta-potential of the PEGylated (or sterically stabilized) SPIONs should be close to zero. However, the use of amino-groups within the coating may result in a slightly positive zeta-potential, while after radiolabelling the nanoparticles they may present a slightly negative net surface charge.

Colloidal stability

The colloidal stability is defined by particles remaining suspended and dispersed in a buffer solution. The stability of the radiolabelled nanoparticles injected in the body is of major importance for a time sufficient to fulfil the purpose and can be studied by incubating the SPIONs in solutions with different ionic strength or serum. SPIONs can be visualized by TEM to confirm the integrity of the formulation and that is dispersed; no aggregation. The stability of the radiolabelled SPIONs can also be monitored by instant thin layer chromatography (ITLC) or paper-chromatography using an appropriate buffer solution as solvent.

Radiolabelling

When developing radiolabelled nanoparticles for SLN imaging, either by SPECT or PET, there are several parameters that need to be considered. The choice of the radionuclide often depends on the availability, chemistry and physical half-life suitable for measurements within the desired time frame. The most common radionuclides for SPECT imaging are ^{99m}Tc ($t_{1/2}$ = 6 h) and ^{111}In ($t_{1/2}$ = 2.8 d), and for PET are ^{18}F ($t_{1/2}$ = 109 min), ^{68}Ga ($t_{1/2}$ = 68 min) and ^{64}Cu ($t_{1/2}$ = 12.7 h).

There are several strategies to incorporate or attach the radionuclide to the nanoparticle surface, as presented in Fig. 7. The two main options are either use of a specific chelator suited to the radionuclide or direct radiolabelling. When a chelator is used, this should form a stable bond and withstand the physiological conditions in vivo. It should not affect the size of the nanoparticles or its pharmacokinetic properties (e.g. clearance from the injection site or uptake in the SLNs). Direct radiolabelling means that the radionuclide forms a strong bond to the surface of the nanoparticles, which contains reactive amino- groups or associates to the metal oxide core by adsorption. The major advantage of this technique is that the labelling can be reduced to a one-step process, while the physical properties of the nanoparticles are minimally affected.

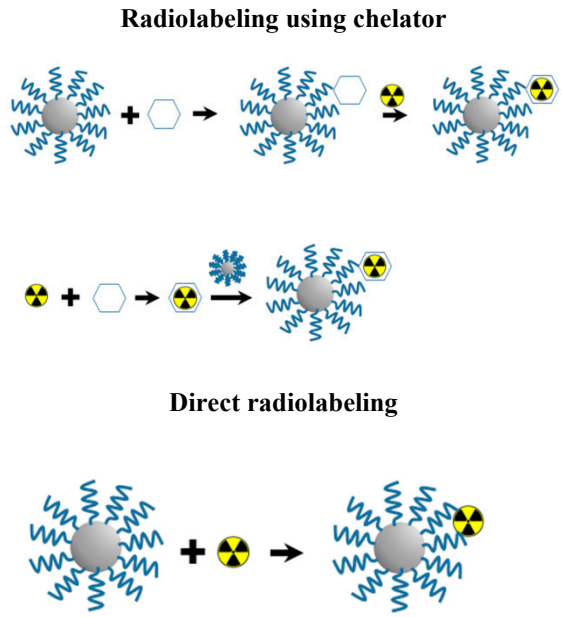

Fig. 6
The general strategies for radiolabelling SPIONs.

Radiochemical purity

Nanoparticles or colloids approved for clinical use are conjugated using kit chemistry for radiolabelling, followed by quality control using ITLC. According to EANM and SNMMI practical guidelines for lymphoscintigraphy a radiochemical purity (fraction of radioactivity incorporated in the chemical composition) greater than 95% is recommended.

Imaging

A part of the breast cancer and malignant melanoma diagnostic examination is to localize and harvest the SLN's for biopsy. The patients are injected with radiolabeled colloids prior surgery. Imaging has an important role in verifying the tracer uptake and localizing the SLN's.

The ideal imaging modality can identify the SLNs and discriminate between normal and metastasized nodes *in vivo*. None of the current imaging modalities are sensitive enough to replace SLNB and histology, however by developing new

tracers (imaging probes) and using hybrid imaging modalities with the right settings we may come closer to our goal. Here are described the imaging modalities used for SLN imaging with their strength and weaknesses in combination with different tracers. In Table 4 are summarised the characteristics of the different imaging modalities used in this thesis.

Lymphoscintigraphy

Until recently, the gold standard was planar scintigraphic imaging, performed with standard gamma (Anger) camera, 1-3 h after subcutaneous or intradermal injection of radiolabeled colloids. When the patients are placed in the camera, γ-rays pass through the collimator holes and interact with the sodium iodine [NaI(Tl)] detector crystals. Consequently, scintillation light is emitted and collected by an array of photomultiplier tubes (PMT's) for read-out. The signal is then converted to planar images using computer software. The system performance highly depends on the physical collimation.

EANM recommends low energy, high resolution or ultrahigh resolution collimators (FWHM at 10 cm is about 5-7 mm).[46] If ^{99m}Tc-labeled colloids are used as tracer, the energy window is set to 15 or 20 % centred on the 140 keV peak. Dynamic series or 5-minutes static planar (anteroposterior and lateral) images are acquired (256 x 256 matrix) over the body region where the SLN is expected. Because lymphoscintigraphic images lack morphological details, a ^{57}Co flood source is placed below the patient (on the frames of the posterior camera head) and a transmission image is acquired to outline the body contours and helps the physicians to locate the SLN's. The lateral emission images help the physicians to estimate the depth of the node in patients.

SPECT/CT

To overcome the limitations in planar images, absence of anatomical landmarks and poor spatial resolution, standard Anger cameras often have been replaced with hybrid SPECT/CT systems. SPECT is equipped with rotating camera heads and acquires multiple projections around the patient. These projections are processed in an iterative reconstruction algorithm to obtain a set of transversal two-dimensional images that form a 3D volume. In addition, a CT scan is performed for attenuation correction of SPECT images and to provide anatomical details to the fused SPECT/CT images. The high-resolution images are displayed using 3D viewer software. Using technique has a higher detection rate for SLN's in near proximity of the injection site was reported in comparison with planar imaging.

PET/CT

PET/CT is a functional imaging modality that enables visualization of metastatic involvement in SLN's using β^+-emitting radiopharmaceuticals such as ^{18}F-FDG. The tracer is injected intravenously and visualizes the metabolic activity in SLN's, unlike from the previously described method where the radiolabeled colloids are more or less "mechanically" trapped within the SLN's. Initially PET/CT using ^{18}F-FDG was thought to be a promising method for staging the breast cancer and malignant melanoma, but proved to have low sensitivity for lesions < 5 mm (25-60 %), mainly due to the low spatial resolution of the system, and thereby is less sensitive than SLN biopsy (SLNB). On the other hand, ^{68}Ga- and ^{64}Cu-labeled SPIONs have been proved to be promising probes to accurately identify and localize the SLN's *in vivo* using preclinical μPET/CT, as presented in Paper III and V.

Standard PET systems consist of several rings of detector crystals coupled to PMT's that surround the patient injected with a β^+-emitting radiopharmaceutical. When the emitted positrons lose their kinetic energy, interact with electrons in tissue and two 511 keV annihilation photons are emitted in nearly opposite direction. These two γ-rays interact near-simultaneously in two detectors on the opposite side of the detector ring. The line in space connecting these two detectors is called for line of response (LOR). The number of coincidences along each LOR is stored in a computer and the projections are used to produce set of transverse images of the activity distribution in patients.

By using annihilation coincidence detection, instead of physical collimation as in SPECT, a higher sensitivity and better spatial resolution is obtained. In PET, the spatial resolution is limited by 1) the intrinsic spatial resolution of detector crystals, 2) the distance travelled by the positron before annihilation and 3) the fact that annihilation photons are not emitted in exactly 180 degrees from each other. To further enhance the spatial resolution; newly developed PET systems are using semiconductor detectors instead of scintillation crystals where each detector area corresponds to one pixel in the image.

The main benefits of this technique are the high sensitivity and accurate activity quantification. PET is also often used complementary with a CT for anatomical information. There are also commercially available PET-MR systems for simultaneous functional/anatomical imaging.

MRI

Magnetic Resonance Imaging (MRI) is a non-ionizing diagnostic imaging tool for retrieving functional and anatomical information. The contrast in MRI images is

obtained using the advantage of different relaxation mechanisms called T1, T2 and T2*. When exciting the desired imaging volume using a radiofrequency pulse (RF) the protons (spins) in the system will get different energy levels. The return of this system to its equilibrium is based on the relaxation properties of the tissues. T2* is a dephasing relaxation of the spins that comes from the inherent T2 of the tissue and the inhomogeneity of the system. In our studies we have used superparamagnetic nanoparticles to induce a large T2* relaxation in the site of the interest. This will lead to a signal loss (called susceptibility effect) in our images.

Table 4

Medical imaging and ex-vivo imaging techniques. PC stands for preclinical and C for clinical systems. Adapted from Rudin M. Molecular Imaging. Basic principles

Techniques	Morphology and/or Functional	Radiation type /Energy	Temporal resolution	Spatial Resolution	Sensitivity	Quanti-tative
MRI	M/F	radio-frequency waves	min – hours	high 100 μm	Low in comparison to SPECT and PET (10^{-3} – 10^{-6} M)	
PET	F	annihilation photons	s – min	1-2 mm (PC) 3-5 mm I	10^{-11} – 10^{-12} M	yes
Planar Scintillation camera	F	γ	min	5-15 mm depending on physical collimation	10^{-9} – 10^{-11}	no
SPECT	F	γ	min	0.5-2 mm (PC) 5-10 mm I	10^{-9} – 10^{-11} M	yes
CT	M/F	x-rays	min	50-200 μm	10^{-3} M	
Optical – NIR	F	visible light or near infrared	s – min	2-4 mm	High 10^{-11} – 10^{-12} M	no
Optical-CLI	F	light in UV/ blue and visible range	min	2-5 mm	10^{-9} – 10^{-12}	yes
DARG	F	α, β	Hours-days	50 μm	10^{-9} – 10^{-11}	yes

Autoradiography

Autoradiography is the best tool to produce two-dimensional images of the activity distribution in thin biological samples used for small-scale dosimetry. Generally, autoradiographic film or photographic emulsions are used, where the samples are exposed and the development of the tissues is studied using high resolution light microscopy. The spatial resolution is only limited by the 0.1-0.4 μm size of the silver halide crystals comprising the detection medium. The main drawbacks of these techniques are the non-linear response to different levels of activity in the samples and the low sensitivity which may require long exposures times. In addition, the non-uniformity of the manually applied emulsions may lead to artefacts. Therefore, in applications where about 100 μm in spatial resolution is sufficient, storage phosphor screens producing quantitative images are preferred. In Paper I, II and V a commercially available digital autoradiography system (Biomolex, Oslo, Norway) was used, based on a semiconductor double-sided silicon strip detector (Hamamatsu Photonics, Hamamatsu City, Japan) with an intrisnic resolution of 50 μm.

Optical imaging

Near-infrared fluorescence (NIRF)

The NIRF molecular imaging has a high potential to be used as standard technique for intraoperative detection and visualization of SLNs for biopsy. This technique requires subcutaneous or intradermal injection of a fluorescence dye that can be excited at NIR wavelengths of > 760 nm and has emission between 700-900 nm. The imaging device comprise of an excitation light source (LED diode), optics and a charge-coupled device (CCD) detector to register the collected light. The signal from the detector is reconstructed using computer software to form a 2D image or color video in real-time of the field of. The penetration depth depends on the fluorescence dye, the sensitivity of the device and tissue type to be imaged; generally is in range of 2 – 4 cm.[47-49]

To date, the non-specific ICG is the only FDA approved NIRF agent available for clinical use. Efforts have been made to conjugate these agents to small molecules, mannose-binding proteins or antibodies to increase.[50] However, the quantum efficiency of ICG is reported be very low (0.3 % yield at 805 nm in water) in comparison with new fluorophores or quantum dots (~ 10 – 80 % yield). Ohnishi et al. reported a threefold increasing of "brightness" and the agent retention in SLNs by conjugating the ICG with human serum albumin.

Other NIRF probes of interest for small animal imaging and potential to translation into the clinic are polymethines (e.g. Cy 5.5 and Cy 7), boron-

dipyrromethene derivatives, Nile blue analogs, oxazyne dye AO1987, and activable probes, QD with tunable NIRF emission respective upconverting nanoparticles.[50]

NIRF-guided SLN biopsy is presented to be a better option than use of blue dye, due to the increased tissue penetration; less toxic and lack of staining on the patient skin.[51]

Cherenkov Luminescence imaging (CLI)

Recent development in optical imaging enables visualizing Cherenkov radiation (CR), light emitted when electrons travelling through tissue with a speed faster than the speed of light. The UV and blue light in the visible spectrum is captured using a deep-cooled and highly sensitive CCD camera and the images are reconstructed using computer software.

Several studies have been conducted and many commonly used radioisotopes were evaluated for CR production.[52-53] The threshold energy to produce CR was calculated to be 263 keV in water (refractive index dependent). For commonly used radionuclides in nuclear medicine, the number of photons produced per decay in decreasing order is: ^{90}Y, ^{68}Ga, ^{15}O, ^{11}C, ^{124}I, ^{89}Zr, ^{18}F and ^{64}Cu.[54]

The major advantages of this technique are that use tracers already approved for nuclear medicine. The imaging technique is cheap in comparison with the other techniques and is relatively easy to implement in a clinical environment. Within preclinical imaging, CLI has much higher animal through-put in comparison with PET and SPECT imaging modalities. However, the penetration depth and the short half-life of the radionuclides producing the signal are challenging.[55]

5. The present investigation

SPIONs

SPIONs used in **Paper I – Paper V**, were produced with precipitation of alkaline solutions containing mainly F_3O_2 by Genovis AB and generously donated for further characterization, functionalization and development as a multimodal agent in vivo. The monodispersed spherical cores were coated with polyethylene glycol whose structure includes primary amino groups. This coating prevents aggregation and enables conjugation with fluorophores and radionuclides; in addition, it avoids serum protein adsorption and immune response which facilitates an increased half-life in vivo. The PEG is FDA approved for biomedical applications, drug formulation and functionalization.

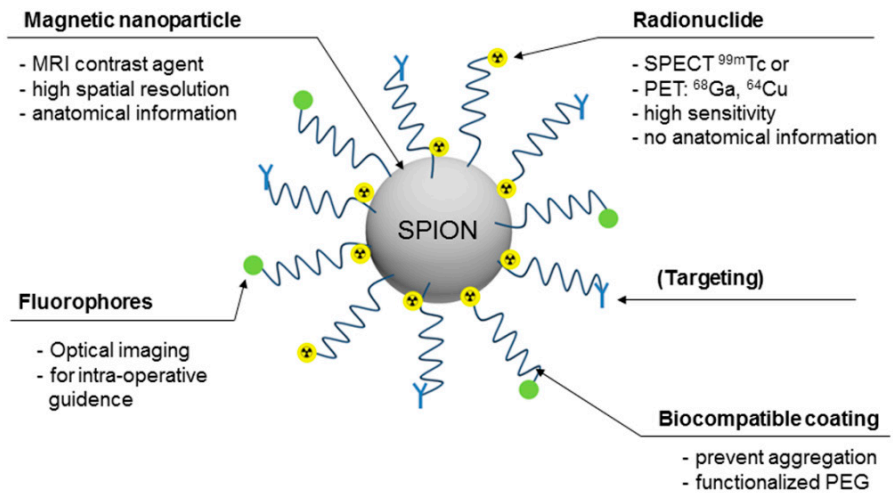

Fig. 7
Concept image of SPIONs.

The physical characterization of the SPIONs

Size

The most significant benefit of SPIONs in comparison to other nanoparticles is that there can be produced in a small size range, close to the optimal diameter for fast transport through the lymphatic system and accumulation in lymph nodes.

Strand and Persson (1979) investigating the uptake of different radiolabelled-colloids in the parasternal lymph nodes of rabbits found that the optimal particle size for SLN detection is in a range of 10-20 nm.[21]

Strand and Persson also demonstrated that there is a strong correlation between the size and absorption/retention of the radiolabelled colloids in SLNs after subcutaneous injection. Small colloids of less than 5 nm in diameter are mostly absorbed in blood capillaries. Nanoparticles of size in the range 5- 100 nm are absorbed in lymphatic vessels and are retained in lymph nodes. Larger nanoparticles, over 100 nm in diameter, have a slower clearance from the injection site, with high probability to be retained in the interstitial space. However, larger nanoparticles that enter the SLNs are trapped in the reticular mash within the medulla and the probability that they will be transported further, to the non-sentinel, second node. Furthermore, after studies conducted in both animals and humans Bergqvist reported that the optimal nanoparticle size for lymphoscintigraphy is in range of 10-20 nm.[21, 29]

In more recent studies, Kjellman et al. (2014) compared the uptake of SPIONs of three different diameters 15 nm, 27 nm, and 58 nm in SLNs and show that the 15 nm particles were accumulated both faster and in higher concentration than the SPIONs of 27 nm and 58 nm in diameter, in accordance with previous observations.[56]

For **Paper I – Paper V**, SPIONs with diameters of about 15 nm were proposed for the experiments. The size of the SPIONs was measured using TEM (Philips TM 10) and DLS (Malvern Zetasizer Nano with clear disposable cells) and found to be 14 nm ± 2 nm and 18 nm ± 3 nm, respectively, in water and after incubation in human serum. It was expected that TEM slightly underestimate the real size of the SPIONs due to the sample preparation (drying) whilst DLS may slightly overestimate the real size because the salt concentration of the medium can induce an electrical double-layer around a charged particle in aqueous. In addition, the PEG "hairy layer" may also induce uncertainties in measurements, which imply to that no absolute value can be obtained.

Charge

The surface charge of the SPIONs was determined by zeta potential measurements which shown that USPIOs coated with amino-PEG were slightly positive at pH 4-

6, with an isoelectric point of 6.2. On the other hand, radiolabelled, ^{99m}Tc-SPIONs were found to have a slightly negative surface charge (- 5 mV) in the pH range 5-7, like most biomolecules in physiological conditions.

Currently, there is no consensus in the literature on what kind of charge the agents should have to achieve a high retention in SLNs. Patel et al. found that negatively charged particles has higher retention in comparison with those of neutral surface charge, which in turn performed better than positively charged particles. In other studies, it was concluded that neutral colloids were cleared faster from the injection site but positively charged colloids had a higher retention rate in the SLNs.[57-59]

In preliminary studies and in **Paper I** found that SPIONs with neutral or small negative charges had a fast clearance from the injection site and high retention in SLNs while positively charged particles probably have a higher affinity for macrophage uptake and RES. However, a large (> 30 mV) positive or negative surface charge may affect colloidal stability by binding with other macromolecules or proteins within the lymphatic fluid.

Stability

The SPIONs were found to be stable in solution with salt concentration > 1.0 M NaCl and common buffer solutions with pH the range 2- 12 which is an important property because some radiolabeling protocols require a low pH in the range 2.5 – 3. The SPIONs were stable in serum for weeks.

If the nanoparticles are not stable, aggregation may occur and the tracer cannot be absorbed and transported through the lymphatic vessels which may lead to a high absorbed dose at the injection site in patients. Failure of conjugation can lead to the release of the radioisotope and entails an unspecific uptake of the activity in organs other than those intended. Unbound ^{99m}Tc, as an example, tends to accumulate in the thyroid and salivary glands. Other issues may occur, for example proteins and other molecules can attach to the nanoparticles after injection in vivo which will affect the size of the nanoparticles, their clearance from the injection site, and their drainage through the lymphatic system.[60]

Magnetic properties, relaxivity, MRI

The SPIONs exhibit superparamagnetic property attributed to the small size (< 20 nm) of the iron oxide core which contains a single magnetic domain with a net magnetic moment. In a magnetic field, the domains re-orient themselves similar to paramagnetic materials, however, the magnetic moment of the SPIONs are much higher than for paramagnetic materials.

SPIONs exhibit a high T2 relaxivity (R2 = 300 $mM^{-1}s^{-1}$, at field strength 0.47 T) in MRI. SPIONs cause a shortening of the transverse relaxation of the spins and local

inhomogeneity in the magnetic field; consequently the signal intensity in tissue containing SPIONs is significantly decreased. The signal intensity loss is dose dependent, and an appropriate pulse sequence is required. This was investigated in preliminary studies (Paper I) using five phantoms containing SPIONs with concentrations of 0.14, 1.4, 14, 145 and 283 µg Fe/mL submerged in a water-filled tank and imaged at the field strength of H = 3 T (Siemens Allegra clinical system for humans). Example images are presented in Fig. 9 using T2 weighted multi-echo FSE and GRE sequences.

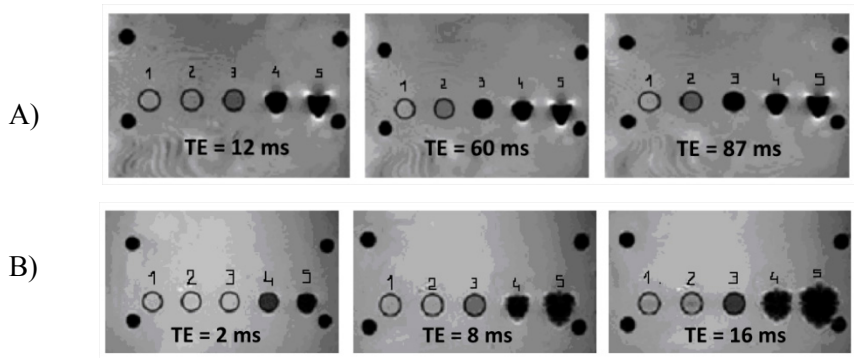

Fig. 9
Relaxation properties of SPION nanoparticles using A) T2 weighted multi-echo FSE and B) GRE sequences. Higher iron concentration corresponds to higher signal loss in the same image at a given TE due to T2 and T2* effects.

The high iron concentration at long TE was shown to lead to blooming artefact in GRE images (Fig. 9, B; phantom 4-5). Therefore, in both animal and future human studies the optimization of the concentration of the injected SPIONs, estimation of their accumulated dose in SLNs, and choice of the imaging sequences are of major importance in order to avoid artefacts. The concentrations administered to animals in this study, were optimized as described in "In vivo evaluation, Administration of the contrast agent".

Radiolabelling and conjugation with fluorophores

^{99m}Tc-SPIONs for SPECT/MR imaging

Technetium is a member of the seventh subgroup of basic elements in the Periodic Table and is a "man-made" (its name comes from the greek "artificial"), or synthetic element. The metastable state ^{99m}Tc (142 keV) decays through 140 keV γ-ray emission with 89% abundance to the ground state ^{99}Tc, with a half-life of $t_{1/2}$ = 6.02. This half-life is long enough to easily synthetize pharmaceuticals, carry out quality control checks, and perform imaging studies shortly after its administration for diagnostic purposes, i.e. to identify SLNs.

^{99m}Tc is available as sodium pertechnetate as the effluent of the ^{99}Mo → ^{99m}Tc generator. In pertechnetate, technetium is in the +7 oxidation state which is not appropriate for synthesis, and it must be reduced to lower (+1, +2, +3, +4, +5) reactive states, either by using traditional reducing agents (e.g. sodium borohydride at pH 11; stannous chloride at pH 3.5; stannouse citrate; concentrated HCl; ferrous sulfate) or organometallic ligands for conjugation.[61] Most of the ^{99m}Tc-radiopharmaceuticals such as ^{99m}Tc-Sestamibi (Cardiolite), ^{99m}Tc-d,l-HAMPAO (Ceretec), ^{99m}Tc-ECD (Neurolite) and ^{99m}Tc-Tetrofosmin (Myoview) are coordinated with ligands, where ^{99m}Tc –forms the core and the ligands are distributed around it, forming the compound.

To synthesize ^{99m}Tc-SPIONs, several different conjugation strategies with radiometals have been reported. Torres et al. developed bifunctional bisphosphonates ligands which were radiolabelled using the dipicolylamine (DPA)-alendronate chelate.[62] Then the ligand was attached to the SPION core. This method can be used only when the SPIONs are not coated with organic polymers. In order to radiolabel for e.g. the dextran-coated Endorem (liver contrast agent) for multimodal SPECT/MRI imaging, the compound must be first heated, until the dextran coating is weakly bound to the conjugate and to obtain ^{99m}Tc-DPA-ale-Endorem.[63]

Another approach is to use a covalently bound chelant (DTPA or EDTA) to coat the SPIONs. Zhang et.al (2009) labelled polyethylene-glycol coated gold nanoparticles with ^{111}In using diethylenetriaminepentaacetic acid–thioctic acid (DTPA-TA). However, by using ligands and chelants there will be a small change in size, shape, lipophilicity and even surface charge on the resulting tracer/probe.[64]

Chelant free labelling has been reported by Levy et al (2004), Porta et al (2007), and Cai Weibo using direct conjugation of the radiometals to N-terminal primary amines on a coating surface.

In Paper I, (Madru et al., 2012) labelling efficiency as high as 99 % was demonstrated when conjugating ^{99m}Tc-SPIONs, using a one-step direct labelling method with primary amines (-NH_2) on the coating surface at room temperature. ^{99m}Tc-ions may also have been absorbed through the surfaces of the SPIONs and attached to the core due to the high affinity of the hydroxyl. Briefly, stannous chloride was used as reducing agent in aqueous solution, at pH 3.4. ^{99m}Tc-pertechnetate was added under vacuum condition, stirred for 30 s and filtered with a 0.22 µm Millipore filter. Then the SPIONs were added in sterile water suspension and the mixture was incubated for 60 min at room temperature.

The labelling efficiency (yield) was determined, by two methods. First, using ITLC-SG (Life Science) with 85% aqueous methanol as mobile phase. Secondly, the radiolabelled SPIONs were magnetically filtered using MACS MS columns and a strong magnet (Miltenyi Biotech). The radiolabelled SPIONs were then rinsed with 0.9 % NaCl solvent. In the all the separated buffer solution, the free ^{99m}Tc activity was measured with a dose calibrator (VDC 303; Veenstra Instruments). Using both methods, free ^{99m}Tc was less than 0.1 % after the labelling. ^{99m}Tc-SPIONs showed high colloidal stability, over 95 % after EDTA challenge and incubation in human serum.

^{68}Ga-SPIONs for PET/MR imaging

The half-live of ^{68}Ga is 67.71 min and it decays through 89% positron emission and 11% electron capture. The average positron energy per disintegration is 740 keV (E_{max} = 1899 keV) which may result in a slightly lower spatial resolution than ^{99m}Tc in PET images, however, ^{68}Ga-SPIONs may also enable detection of SLNs with e.g. Cherenkov luminescence imaging.[55]

^{68}Ga is in the 3rd subgroup, group XIII in the Periodic Table and it has a single stable oxidation state in aqueous solution (+ 3) under acidic conditions. It forms stable complexes with ligands containing oxygen, nitrogen, sulfur, phosphonates, hydroxamate, and amine, or with functional groups such as phenolate or thiol. Many studies have demonstrated that the best chelator for ^{68}Ga is 1,4,7,10-tetraazacyclo-dodecane-1,4,7,10-tetraacetic acid (DOTA), which is bifunctional, forming stable complexes with ligands and peptides for clinical use in patients.[63]

However, when Ferreira et al. evaluated several chelant for conjugation with ^{68}Ga they found that p-NO2-Bn-NOTA and p-NO2-Bn-PCTA were relatively inert, while ^{68}Ga-radiolabelled p-NO2-Bn-DOTA had intermediate stability, it was shown that more than 20 % of the ^{68}Ga was disassociated when incubated with apo-transferrin for less than 1 h.[65]

Schiller E et al. (2013) developed ^{68}Ga- and ^{64}Cu – labelled NOTA-human serum albumin for SLN detection.[66] For radiolabelling 0.5 M ammonium acetate (pH 5) was used with a reaction time of 15 minutes at room temperature. The radiolabelling efficiency was determined by ITLC with 0.1 M citrate buffer (pH 5) as the mobile phase and found that the radiochemical yield was over 95 %. A high accumulation of 2.78 %IA ± 0.38 %IA and 6.13 %IA ± 1.13 %IA (at 10 minutes and 60 minutes, respectively, after subcutaneous injection) was found in the SLNs of Wistar rats.

Few studies have been reported with ^{68}Ga-labelled iron oxide nanoparticles. Hofman, developed ^{68}Ga-labelled SPIONs for SLNs detection in patients with prostate cancer.[67]

Burke et.al (2015) prepared silica-coated iron oxide nanorods and labelled them with ^{68}Ga using in one protocol tetraazamacrocyclic (DO3A) as chelant and second protocol tat used a chelator-free conjugation. It was shown that a 97 % radiolabelling efficiency of ^{68}Ga-nanorods could be achieved within 15 min, without using the chelant.[68]

In Paper III (Madru et.al) a chelator-free, one step labelling protocol was developed to conjugate ^{68}Ga-SPIONs for SLNs detection using three different imaging modalities – PET/MR/Cherenkov luminescence imaging. $^{68}GaCl_3$ was eluted from ^{68}Ga/^{68}Ge- generator (IDB Holland) using 0.6 M hydrochloric acid. It is known that at low pH, ^{68}Ga form insoluble $^{68}Ga(OH)_3$ resulting in a low radiolabelling yield. Therefore, sodium acetate, HEPES and ammonium acetate buffer solution were evaluated and the optimal pH was determined to maximize the labelling efficiency. It was found, that amino-PEG coated SPIONs can be labelled with ^{68}Ga in a one-step process using ammonium acetate buffer solution (1 M, pH 5.5) by incubation of the mixture at 50 ºC for 25 min.

The radiolabelling efficiency was determined, in the first instance by ITLC (TEC-control chromatography strips, Biodex, USA) using 0.2 M citric acid as running buffer. The ITLC-strips were analysed using a phosphor imager (Welesley, MA, Perkin Elmer, USA and phosphore storage plates (Multisensitive, Medium, Perkin Elmer, USA). The plates were exposed for 5 min and then analysed with OptiQuant image analysis software (Perkin Elmer, USA). Secondly, ^{68}Ga-SPIONs were magnetically filtered using MACS MS columns and a magnet, in the same procedure described earlier in previous section with the exception that the ^{68}Ga-SPIONs were eluted with ammonium acetate. The radiolabelling efficiency was found to be 97% in both quality assurance techniques. The ^{68}Ga-SPIONs were incubated in human serum for 270 min and were found to be stable.

^{64}Cu-SPIONs

^{64}Cu- is reactor or cyclotron produced radionuclide ($t_{1/2}$ = 12.7 h; β^+ = 0.653 MeV, 17.4 %; β^- = 0.578 MeV, 39 %; EC 44 %) and is a commercially available PET imaging agent. It is well suited to labelling antibodies, antibody fragments, peptides and nanoparticles. ^{64}Cu (II) is the most common oxidation state and easily binds with nitrogen donors. Therefore, the frequently used chelators are NOTA, DOTA or the phosphonate-armed chelators such as CB-TE2P and CB-TE1A1P, respectively, for fast labelling of peptides at temperature ~40 ºC.[69-70]

Torres et al. reported a method for labelling iron oxide nanoparticles with ^{64}Cu using dithiocarbamatebisphosphonate (DTCBP) as bi-functional chelator. The ^{64}Cu-DTCBP-SPIONs were found to be relatively stable for in vivo applications such as like SLN imaging in small laboratory animals.[71]

In a study by Glaus et al. ^{64}Cu-DOTA-mSPIOs (micelle-coated SPIOs) were prepared.[72] First, the DOTA-mSPIOs were conjugated by adding the mSPIONs to DOTA-NHS-ester in PBS (pH 7.5) and left overnight at 4 ºC. Then, dialysis with 2L of phosphate buffer was used, over 48 h, to separate the DOTA-mSPIOs from the excess of DOTA-NHS-ester. Secondly, the DOTA-mSPIOs were incubated with ^{64}Cu in ammonium acetate buffer (0.1 M, pH 5.5) for 1 h at 37 ºC. A radiolabeling yield of 94 % was found and incubation in mouse serum of the agent indicated a high in vitro stability. In a study by Zhou et al. the CuS nanoparticles were formed through incorporating the ^{64}Cu- into metal matrices for imaging and photothermal ablation of tumours.[73] Chelator-free complexes have also been developed by Petersen et al. in which the ^{64}Cu was incorporated into liposomes.[74] However, the methods presented above are very time consuming.

Therefore, **in Paper V** chelator free ^{64}Cu-SPIONs were developed as a novel PET-MRI imaging agent. The amino-PEG coated SPIONs were incubated with $^{64}CuCl_2$ in ammonium acetate solution (0.1 M, pH 5.5), at room temperature. After 10 min, the ^{64}Cu-SPIONs were filtered using MACS columns and a magnet. The magnet helped to retain the nanoparticles in the column and thereafter when it was removed, the ^{64}Cu-SPIONs were eluted in ammonium acetate. The labelling yield was determined with the ITLC method and found to be 97 %. ^{64}Cu-SPIONs were shown to have good stability (> 95 % after 24 h), tested in both buffer solution and mouse serum.

In vivo studies

The animal studies in Paper I-IV were conducted in accordance with local and national regulations approved by the Local Ethics Committee for Animal Research, Lund, Sweden. The animal procedures were performed under anaesthesia by inhalation of 2-3 % (rats) and 1-2 % (mice) isoflurane-air mixture. The animal study in Paper V was conducted at Brookhaven National Laboratory in accordance with guidelines from the Institutional Animal Care and Use Committee and with the *Guide for the Care and Use of Laboratory Animals* from the National Institutes of Health.

Animal models

To evaluate the in vivo stability and feasibility of SPIONs for SLN detection laboratory animals, rats (Paper I-IV) and mice (Paper V) were used. These rats were healthy white male Wistar rats weighing 150-200 g and were purchased from Charles River, Germany. The lymphatic drainage and location of the SLNs in rats is well documented in the literature.[75] The sizes of the lymph nodes are suitable for imaging with the different imaging modalities used in this study. The mice were of type C56 black, female, 3 months old obtained from Charles River Laboratory.

Administration of the contrast agent.

There are two different routes of administration of SPIONs to detect the SLNs. First, injecting the SPIONs intravenously in the rat or mouse tail. Blood vessels leak macromolecules including SPIONs into the interstitial tissue where they are phagocytized by macrophages and transported into the lymph nodes through the lymphatic system. This method is more useful for dextran-coated SPIONs because PEGylated SPIONs are less recognized by the macrophages.

In **Paper I – Paper V**, the second, passive targeting method was selected, for administration. This method mimics more closely the clinical application by injecting the SPIONs subcutaneously or intradermally in the dorsal side of the right hind paw. This method permits the study of the clearance rate from the injection site, and drainage and retention of the SPIONs in the first, popliteal lymph node, located behind the knee in rats and mice.

The administered dose (or “iron” concentration) was optimized for the equipment used for MRI imaging in order to avoid artefacts. The optimization included both phantom studies as shown in Fig. 9 and animals injected with different concentrations or radiolabelled SPIONs.[56] **In Paper I and II**, SPIONs

corresponding to ~ 0.2 µg (iron) was injected and imaged using 3T MRI, Philips Achieva, equipped with a Sense Flex Coil. **In Paper III**, ^{68}Ga-labelled SPIONs corresponding to ~ 0.13 µg iron were administered to the animals in order to be imaged using a 9.4 T Agilent Palo Alto system equipped with a transmit/receive 72 mm inner diameter volume coil (Rapid Biomedical, Rimpar, Germany). In Paper V, 1.4 µg Fe/mL was injected in the hind paw of C57BL/6J mice and imaged with Bruker Biospec 9.4 T MRI scanner, using ParaVision 5.0 image viewer software.

Biodistribution of the radiolabelled SPIONs

The biodistribution of the SPIONs depends on the physico-chemical properties, the radioactive isotope and the molecules attached to the surface of the nanoparticles. Furthermore, the biodistribution is also affected by the interaction of the nanoparticles with proteins or other molecules in tissue and lymphatic fluid. Nanoparticles may also be metabolized by monocytes and macrophages. To avoid recognition and increase the biological half-life polymer polyethylene glycol (PEG) coating material was used. Generally, small nanoparticles tend to be cleared through the kidneys while large nanoparticles (~ 100 nm) accumulate in liver, spleen and are more likely to be cleared through the faces.

The same type of SPIONs were used throughout the all five reports, (**Paper I – Paper V**) but labelled with different radioisotopes (^{99m}Tc, ^{68}Ga and ^{64}Cu) and fluorophore (Alexa Fluor 647, Molecular probes, Life Technologies).

The animals were injected subcutaneously with the radioactive probes (0.05-0.07 mL) in the right hind paw. The amount radiolabelled SPIONs clearance from the injection site was measured to be 20-30 % IA, at 3-5 h after the injection. The biodistribution of the different radiolabelled probes was also found similar because no chelators were used and the radiolabelling does not affect the SPIONs size significantly.

The highest uptake and retention in SLNs was obtained using ^{99m}Tc-AF-SPIONs, followed by ^{99m}Tc-SPIONs and then ^{68}Ga-SPIONs (Table 5). However, the animals injected with ^{68}Ga-SPIONs could be followed by imaging only up to 3 h post injection, due to the shorter half-life of this radionuclide.

Table 5
Comparison of the biodistribution of different agents injected subcutaneously in white Wistar rats. After the last imaging session, 5h and 3 h (^{68}Ga) p.i.,organs of interest were resected, weighed and measure for activity.

Wistar Rats	^{99m}Tc-SPIONs (% IA / g) 5 h p.i.	^{99m}Tc-AF-SPIONs (% IA / g) 5 h p.i.	^{68}Ga-SPIONs (% IA / g) 3 h p.i.
Popliteal (SLN)	211 ± 225	330 ± 120	123 ± 67
Illiac	-	150 ± 20	47 ± 5.4
Kidney	0.3 ± 0.08	0.5 ± 0.08	0.05 ± 0.01
Spleen	0.2 ± 0.1	1.3 ± 0.02	0.1 ± 0.04
Liver	1.4 ± 0.7	0.1 ± 0.2	0.3 ± 0.19
Inj site	-	-	39.5 ± 27.1

In **Paper IV**, the biodistribution study of the ^{64}Cu-SPIONs was carried out in C56 black female mice. The ^{64}Cu-SPIONs were administered subcutaneously in the right hind paw, just as in the previous studies on rats. The SLNs and organs of interest were dissected 24 h post injection. It was found that ^{64}Cu-SPIONs were still present and retained in SLNs (4.8%IA/g ±1.73% IA/g), spleen (1.3%IA/g ± 0.3%IA/g), kidney (6.3%IA/g ±0.96 %IA/g), liver (11%IA/g ± 1.88%IA/g), and at injection site (17.52%IA/g ± 1.92%IA/g). In addition, ^{64}Cu-SPIONs were found in the gastrointestinal tract, in the small and large intestine, 27%IA/g ± 2.86%IA/g respective 23%IA/g ± 1.92 %IA/g, shown to be the main clearance route from the body.

Multi-modality imaging with SPIONs

In order to overcome the limitations of single imaging modalities such as poor spatial resolution, low sensitivity and limited signal penetration in tissue, multi-modality imaging techniques such as PET/CT, SPECT/CT, PET/MR and bed-side optical imaging systems have been developed. These combined techniques require a single imaging probe that can be detected simultaneously by each of the combined imaging modalities to avoid injecting patients with multiple tracers and contrast agents (e.g. ^{18}F-FDG for PET and Gd-DTPA for MRI). SPIONs have a native MRI contrast due to the monodisperse iron oxide core. In addition, the PEG coating enables attachment of radionuclides or fluorophores as it was described above.

MR-Optical

Fluorescein- or rhodamine-SPIONs were the first dual-modality imaging probes reported. However, conventional fluorophores emitting in the visible spectra are of little value in vivo imaging. Near-infrared (NIR) dyes however, emit in the 700-900 nm wavelength region where blood and tissue have lower absorption and the emitted light can be detected using relatively cheap, bed-side optical imaging devices or directly integrated in MRI detection systems.

Although NIR fluorescence imaging is a very powerful tool due to the high sensitivity and specificity of the probes, no anatomical information is provided by this technique. Therefore, the interpretation of results may be challenging if the technique is not combined with high resolution MRI or CT; often MRI is preferred over CT because it does not involves ionizing radiation.

In the last decade much research was focused on development of combined MRI-Optical imaging probes. The majority of the probes developed include SPIONs, Gd^{3+} conjugated with NIR-fluorophores, or quantum dots (QDs).[76]

Zhou et al. developed a new a NIR-830 dye conjugated to iron oxide nanoparticles with core size diameters of 10 nm. The probe was shown to be feasible for visualizing SLNs in mice with both MRI and an optical imaging system up to 60 min after the administration of the probe. [77]

Bump et al. developed silica coated iron oxide nanoparticles conjugated with Cy 5.5. Nude mice were injected with the developed probe and imaged with MRI and, optical imaging and the axillary lymph nodes were resected for histological analysis. The probe was shown to be accurate for identification of the SLNs with both imaging modalities.[78]

In **Paper II** it was demonstrated that Cy5.5 conjugated SPIONs can accurately identify SLNs lymph nodes in tissue at 2 cm depth. (Fig. 10) The probe was administered into the hind paw of white Wistar rats, shaved in the region of interest. The MRI anatomical images clearly visualized the lymphatic drainage and SLNs. The nodes could be resected using optical imaging and the distribution of the Cy 5.5-SPIONs could be visualized using fluorescence microscopy. Most of the Cy 5.5-SPIONs were found in the subcortical and medullary sinuses, extracellularly. In addition, the developed probe also enabled attachment of additional tracers such as radionuclides for SPECT or PET imaging.

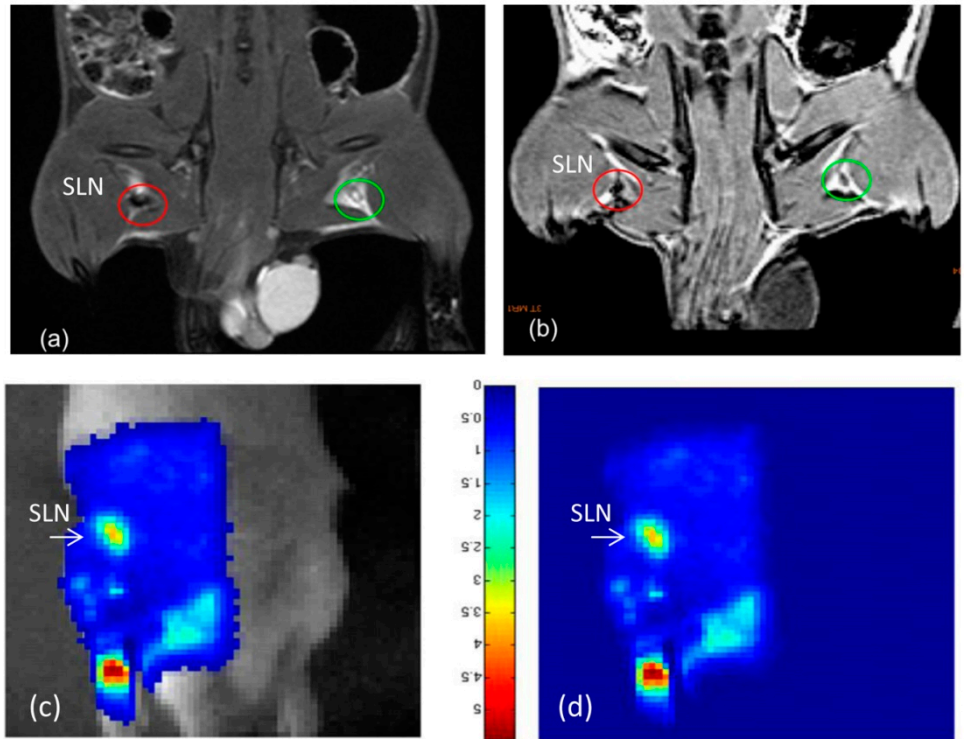

Fig. 8
MR and opical images of white Wistar rats after subcutaneously administrated 99mTc-SPION-Cy 5.5.

MR – SPECT or MR – PET

The major limitation of the MRI technique is its low sensitivity and signal-to noise-ratio. Therefore, low uptake of contrast agents, including SPIONs, makes detection or quantification in vivo difficult. However, SPECT or PET is very sensitive, nanomolar or lower concentrations of tracer can be visualized. Therefore, radiolabelled-SPIONs carrying even a low specific activity can enable the detection of small uptakes of the contrast agent in organs or tissue of interest. SPECT or PET allows detection and quantification of the accumulated contrast agent in SLNs while the high- resolution MRI allows could identification of metastases in the lymph nodes.

Currently available systems using simultaneous image registration, result in "perfect" spatial registration of functional and morphological MRI-PET images.

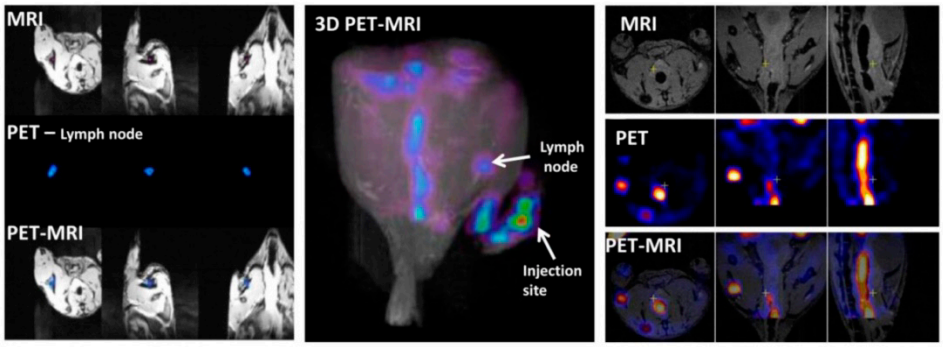

Fig. 9
Example PET, MRI and fused PET-MRI images of mice injected with 64Cu-SPIONs in the right hind paw. The agent rapidly accumulates in lymph nodes (left image, 30 min post injection). The signal loss in tissue containing 64CuSPIONs in MRI is dose dependent (right image, 24 h post injection).

In **Paper V** the feasibility of using ^{64}Cu-SPIONs for visualizing SLNs by simultaneous PET- MRI acquisition and imaging using a Varian large bore 9.4 T MRI system (equipped with commercial Insight birdcage coil) and integrated RatCAP PET system was demonstrated. The mice were injected subcutaneously with ^{64}Cu-SPIONs in the dorsal hide paw. The accumulation of the ^{64}Cu-SPIONs in the popliteal lymph node could be visualized within 10 min after the injection, and the biodistribution of the probe could be followed up to 24 h (Fig. 11).

Lee at al. developed polyaspartic acid coated SPIONs (hydrodynamic diameter ~45 nm), conjugated with cyclic arginine-glycine-aspartic (RGD) peptides and ^{64}Cu-DOTA for PET –MRI imaging of tumour integrin expression. This dual modality imaging technique can lead to early tumour detection due to the increased sensitivity and high resolution of the 3D tomographic MRI images. In addition, using simultaneous image acquisition, the motion and organ deformation between imaging sessions is eliminated. Furthermore, the accurate co-registration of MRI and PET images can also be used to correct for partial-volume effects in PET images.[77]

MR – PET – Cherenkov Luminescence Imaging

The most commonly used optical imaging techniques for small animal imaging are based on fluorescence and bioluminescence. The translation to clinical applications of these techniques is limited by the depth-penetration of the light and the toxicity of most fluorophores. In this respect, Cherenkov luminescence imaging may be a door-opener, using already approved tracers i.e. ^{68}Ga, ^{89}Zr, ^{18}F for diagnostic PET imaging, and for e.g. guidance of SLN surgery.

In the field of small animal imaging, this technique has the advantage of high through-put compared to PET or SPECT imaging during studies of the uptake of radiotracers or follow-up therapies.

In **Paper III** (Madru et al.) it was demonstrated that ^{68}Ga-SPIONs injected into the hind paw of white Wistar rats can be visualized with MR, PET and CLI (Fig. 12). The MRI provides the high-resolution 3D anatomical images which may enable differentiation between normal and diseased lymph nodes, PET is highly sensitive, and CLI can be used as surgical guidance for SLN biopsy.

One of the challenges of using CLI is that the amount of light emitted is small in comparison to fluorescence or bioluminescence. However, there is less non-specific background signal in the CLI technique. Deep tissue imaging represents a problem because the blue light is highly attenuated by tissues.

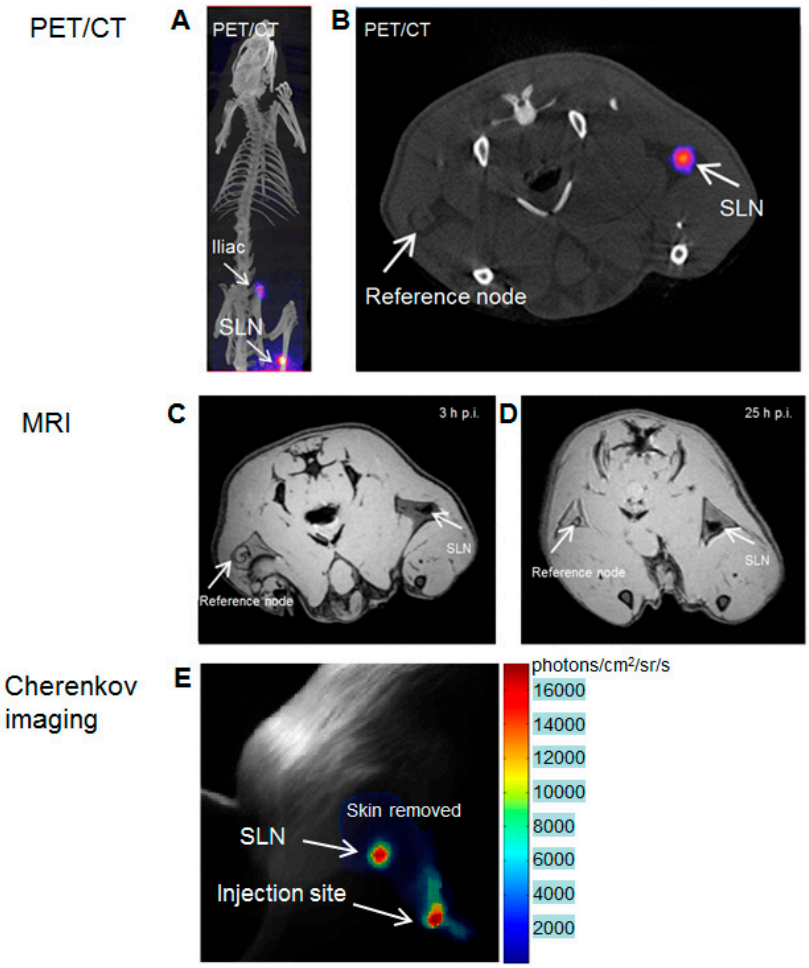

Fig. 10
Multimodal imaging of SLNs in white Wistar rats. A) PET-CT image of the first (popliteal) and second (Illiac) SLN in the animal. B) PET-CT axial image visualizing the uptake of 68Ga-SPIONs in an SLN in comparison with a contralateral reference node. C) Axial MRI image corresponding to B and visualizing the SLN and reference node. D) Axial MRI slice of the same animal, imaged 25 h p.i. E) CLI of the white Wistar rat, visualizing the SLN and injection site.

Dosimetry

In the last decade much focus has been on developing new radiolabeled agents for targeting and multimodality imaging of SLN's. However, there are few studies reporting about the activity distribution within the SLN. Common mistake is to suppose that there is a uniform distribution of the nanoparticles within the healthy SLN's, often based on MRI and nuclear imaging. In **Paper II**, white wistar rats were injected subcutaneously in the right hind paw with ^{99m}Tc-SPION-Cy5.5 After 5 h p.i. the rats were sacrificed, the SLNs were dissected, and frozen. 20 µm thick coronal sections mounted on microscopy slides. The sections were hematoxylin and eosin (H&E), and DAPI stained respectively for microscopy analysis (Zeiss Axiovert 200M), (Fig.13). Comperatively, in **Paper IV**, ^{99m}Tc-SPION and ^{99m}Tc-Nanocoll were injected in rats according to the same protocol descriebed above. In addition even SLNs from patients injected with ^{99m}Tc-Nanocoll were collected weighed, measured for activity, frozen section were prepeared, monted on microscopy slides, and (H&E) stained. All animal and patient specimens were imaged with DARG (Fig.14)**.** DARG and microscopy images are in good agreement demonstrating the non-homogenous nanoparticles- and activity distribution.

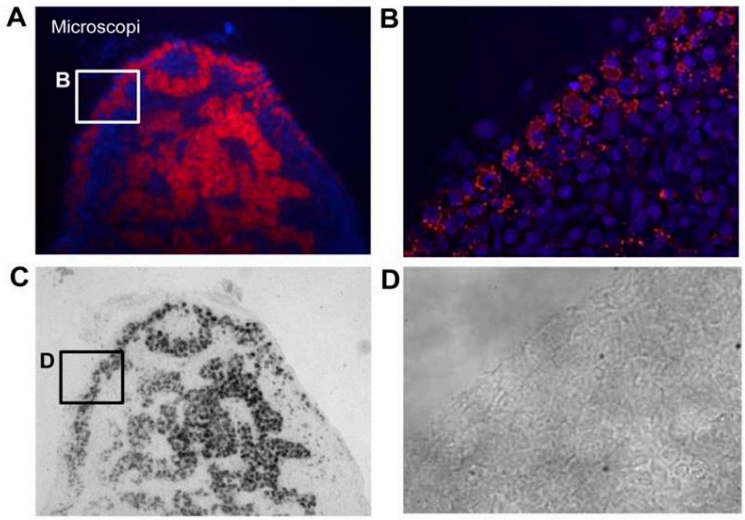

Fig.13 **11**

Microscopy images of frozen-sectioned SLN. A) Coronal section (20 µm) of a half SLN indicating the distribution of the ^{99m}Tc-SPION-Cy5.5 within the SLN. The blue structures are cell nucleus and the red color is light emitted from the Cy 5.5 from the surface of the SPIONs. The nanoparticles are mostly accumulate in the cortex and within the medullary sinuses B) Image visualizing the cortex of the SLN and indicating that the nanoparticles are mostly located extracellulary in comparison with the medullary sinuses where the nanoparticles seems to be located within the macrophages. C) and D) bright field imaging which show the orientation and anatomy.

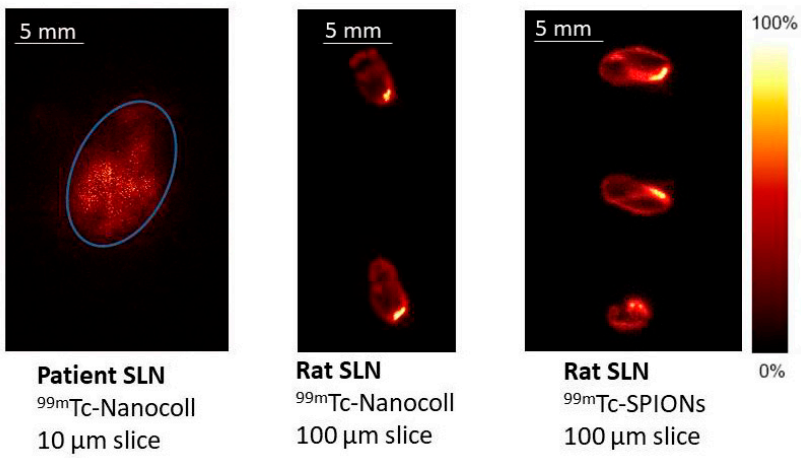

Fig.14 DARG frozen-sectioned SLN and visualizing the activity distribution Left) patient SLN after injection of ^{99m}Tc-Nanocoll. Middle) rat SLN after injection of ^{99m}Tc-Nanocoll and Right) rat lymph nodes after injection of ^{99m}Tc-SPIONs.

The absorbed dose rates in SLNs were calculated from the activity image from DARG images convoluted with a point-dose kernel. The point dose kernels for ^{99m}Tc and ^{68}Ga were simulated with the Monte Carlo code MCNP5 1.60, using the new electron sampling logic option and a voxel size of 50 μm, corresponding to the voxel size of the DARG system. Since data from adjacent tissue were missing, the same image was stacked to get the absorbed dose rate contribution from adjacent tissue. To determine the absorbed dose the time-integrated activity constant, TIAc, (residence time) were determined from dissected SLNs in rats (n=6) at 0, 1, 2, 3 and 5 h. An exponential curve was fitted for the first 5 hours where the maximal uptake of 60% of the injected dose was reached and for the times beyond 5 hours the uptake was considered constant. The physical decay then was added and the TIAc could be calculated. The TIAc were multiplied with the dose-rate images to produce absorbed-dose images. These were then filtered with a Gaussian smoothing filter (σ=1 voxel) and three threshold (ratio of max)-based ROIs were derived, Region1 [0.12-0.25], Region 2 [0.25-0.4] and Region 3 [0.4-1.0]. These ROIs were applied for the dose rate images to calculate the absorbed dose in the various regions.

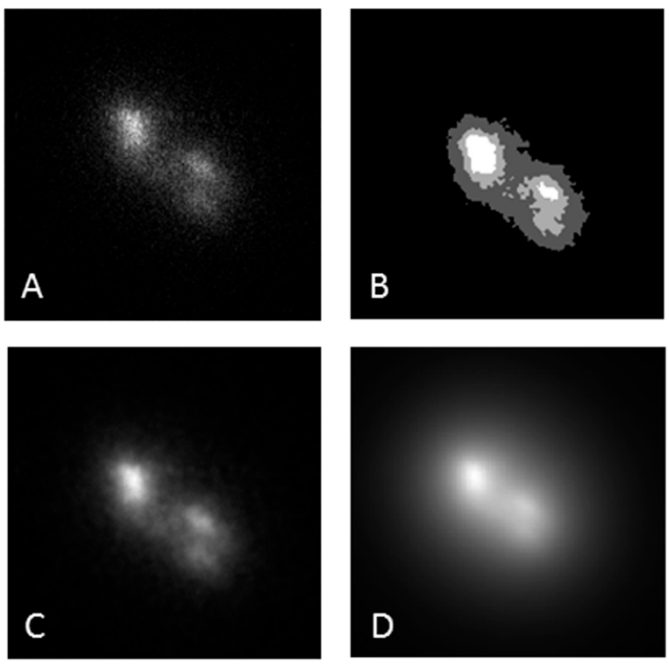

Fig.15 Example DARG image of activity distribution A) in patients, B) ROI, C) Absorbed dose ^{99m}Tc-Nanocoll.D) respectively ^{68}Ga.

Because the activity concentration of the radiolabelled colloids and SPIONs is not homogenous through the entire SLN and the activity concentration can be 2-3 times higher in some small regions than in other regions, the absorbed dose to structures within some regions was found to be approximatively 4 folds higher using small scale dosimetry model and compared to the mean absorbed dose to the whole node. The absorbed dose calculated for the entire lymph node, was concurrent with those reported in the product specifications for ^{99m}Tc-Nanocoll.

It was found that the absoebed dose heterogeneity is somewhat different between ^{99m}Tc- or if ^{68}Ga-SPIONs would be used, resulting in maximal to mean absorbed dose ratio of 2.7 ± 0.3 and 1.6 ± 0.1, respectively, owing to the different emission characteristics, i.e. particle range, **Paper IV**.

Conclusion remarks

- SPIONs have shown to have optimal physical characteristics for transport through the lymphatic vessels. The biocompatible and functionalized coating enables direct radiolabelling with different radionuclides for SPECT, PET, MRI and Optical imaging
- ^{68}Ga-SPIONS has a high potential to be used for intra-operative CLS imaging in clinical application SLN biopsies.
- The use of a single hybrid probe and simultaneous hybrid imaging provides an efficient, complementary integration of quantitation and is expected to improve pre-operative planning and intra-operative guidance for cancer treatments.
- Dosimetry calculations taking in account anatomical information based on high resolution images are important. Common approach of MIRD assuming a homogenous activity distribution it may underestimate the absorbed dose in some regions in SLN.

Acknowledgement

During my PhD studies I have received help and support from several persons, for which I am very thankful. I would like to express my gratitude to all of you and in particular to:

My main supervisor, *Sven-Erik Strand*, who not only supervised me through all my projects but also introduced me to several of his national and international colleagues within our research field. It was a pleasure to work and conduct experiments at Caltech, LA and Brookhaven National Laboratory, NY. I´m so grateful for all ideas we shared, discussed, and wrote about. Thank you for your patient.

My co-supervisor, *Linda Knutsson* for all discussions and your huge support when writing my papers, and abstracts for conferences, always in last minutes. It was a pleasure to have you around during experiments, and so much fun traveling with you.

Michael Ljungberg, who formally was not my supervisor but nevertheless acted as one, thank you for supporting me and encourage me during writing of my thesis.

My co-supervisor, *Freddy Ståhlberg*, for accepting me in the MRI group and take part in your discussions.

Sarah Fredriksson och *Fredrik Ohlsson* and Genovis for supporting my research and providing the nanoparticles to my projects. Thank you!

Tomas Olsson and *Lennart Bergqvist* for supporting my projects and providing radionuclides for labelling of nanoparticles. Thank you!

Dr. Christian Ingvar, it was a great pleasure to discuss our projects with you. Thank you for your help in conducting the clinical study.

Special thanks to *Karin Wingårdh*, who supported me and helped me when I was a novice.

To *Thuy Tran, Bo Holmqvist, Gustav Grafström, Rene In 'T Zandt, Adnan Bibic, Johan Olsrud, Jimmy Lätt, Carina Siversson, Jonathan Siikanen* for help during experiments.

All of the *co-authors* of the papers for providing expertise in different fields.

All my friends and colleagues for pleasant company and help in many different areas, *Oskar Vilhelmsson Timmermand, Anders Örbom, Pontus Kjellman, Suaad Meerkham, Sophie Eriksson, Erika Elgström, Susan Evans-Axelsson, Ronnie Wirestam, Katarina Sjögreen-Gleisner, Lena Jönsson, Sigrid Leide, Emelie Lind, Filip Szczepankiewicz, Björn Lampinen, Mikael Peterson, Gustav Brolin, Johan Gustafsson, Karin Markenroth Bloch, Peter Mannfolk, Anders Sandell,* and colleagues from Lund University Bioimaging Center, LBIC, Skane University Hospital, Oncology Department, MRI group, Radiation therapy and Medical Radiation Physics in Malmö and Lund.

Special thanks goes to my *Mom* and *family, Etienne and William* who often joined me to work, were so understanding, and such a good kids during my meetings.

References

1. Cancerfondens rapport, 2016

2. Hirche C, Mohr Z, Kneif S, Hünerbein M. The role of nodal staging in breast cancer. Past, present and future. Minerva Chir. 2010;65(5):537-46.

3. Viale G, Sonzogni A, Pruneri G, Maffini F, Masullo M, Dell'Orto P, Mazzarol G. Histopathologic examination of axillary sentinel lymph nodes in breast carcinoma patients. J Surg Oncol. 2004;85(3):123-8

4. Giammarile F, Alazraki N, Aarsvold JN, Audisio RA, Glass E, Grant SF, Kunikowska J, Leidenius M, Moncayo VM, Uren RF, Oyen WJ, Valdés Olmos RA, Vidal Sicart S. The EANM and SNMMI practice guideline for lymphoscintigraphy and sentinel node localization in breast cancer. Eur J Nucl Med Mol Imaging. 2013;40(12):1932-47

5. Giuliano AE, Kirgan DM, Guenther GM, and Morton DL. Lymphatic mapping and sentinel lymphadenectomy for breast cancer. Ann Surg. 1994;220(3):391-401.

6. Fahy AS, Grotz TE, Keeney GL, Glasgow AE, Habermann EB, Erickson L, Hieken TJ, Jakub JW. Frozen section analysis of SLN in trunk and extremity melanoma has a high false negative rate but can spare some patients second operation. J Sueg Oncol. 2016;114(7):879-883.

7. Alex JC, Krag DN, Harlow SP, Meijer S, Loggie BW, Kuhn J, Gadd M, Weaver DL. Localization of regional lymph nodes in melanomas of the head and neck. Arch Otolaryngol Head Neck Surg. 1998;124(2):135-140.

8. Griffith JF, Chan AC, Ahuja AT, Leung SF, Chow LT, Chung SC, Metreweli C. Neck ultrasound in staging squamous oesophageal carcinoma - a high yield technique. Clin Radiol. 2000;55(9):696-701.

9. Tiguert R, Gheiler EL, Tefilli MV, Oskanian P, Banerjee M, Grignon DJ, Sakr W, Pontes JE, Wood DP. Lymph node size does not correlate with the presence of prostate cancer metastasis. Urology. 1999;53(2):367-71.

10. Curtin HD, Ishwaran H, Mancuso AA, Dalley RW, Caudry DJ, McNeil BJ. Comparison of CT and MR imaging in staging of neck metastases. Radiology. 1998;207(1):123-130.

11. Jain R, Dandekar P, Patravale V. Diagnostic nanocarriers for sentinel lymph node imaging. J Control Release. 2009;138(2):90-102.

12. Nune SK, Gunda P, Majeti BK, Thallapally PK, Forrest ML. Advances in lymphatic imaging and drug delivery. 2011;63(10-11):876-885.

13. Nunez C, Estevez SV, Del Pilar CM, Inorganic nanoparticles in diagnosis and treatment of breast cancer. J Biol Inorg Chem. 2018; Epub ahead of print.

14. Pratt EC, Shaffer TM, Grimm J. Nanoparticles and Radiotracers: Advances toward Radio-Nanomedicine.2016; 8(6):872-890.

15. Michel SCA, Keller MT, Fröhlich MA, Fink D, Caduff R, Seifert B, Marincek B, Kubik-Huch RA. Preoperative breast cancer staging: MR imaging of the axilla with ultrasmall superparamagnetic iron oxide enhancement. 2002;225(2)

16. Pouw JJ, Grootendorst MR, Bezooijen R, Klazen CAH, Bruin W, Klaase JM, Hall-Craggs MA, Douek M, Haken B. Pre-operative sentinel lymph node localization in breast cancer with superparamagnetic iron oxide MRI:the SentiMAG Multicare Trial imaging subprotocol. 2015;88(1056)

17. Skober M, Detmar M. Structuer, function and molecular control of the skin lymphatic system. 2005;5(1):14-19.

18. Choi I, Lee S, Hong Y-K. The new era of the lymphatic system: no longer secondary to the blood vascular system. 2012;2(4)

19. Vainionpää N, Butzow R, Hukkanen M, Jackson DG, Pihlajaniemi T, Sakai LY, Virtanen I. Basement membrane protein distribution in LYVE-1-immunoreactive

lymphatic vessels of normal tissues and ovarian carcinomas. 2007;328(2):317-328.

20. Multhuchamy M, Gashev A, Boswell N, Dawson N, Zawieja D. Molecular and functional analyses of the contractile apparatus in lymphatic muscle. 2003;17(8):920-922.

21. Strand SE, Bergqvist L. Radiolabelled colloids and macromolecules in the lymphatic system. Crit Rev Ther Drug Carrier Syst. 1989;6(3):211-238.

22. Grundmann E and Vollmer E. Reaction patterns of the lymph nodes. 1990; New York: Springer-Verlag. ISBN 0387522883.

23. Alitalo K. The lymphatic vasculature in disease. Nat Med 2011;17(11):1371-1380.

24. Ulrich H von Andrian and Mempel TR. Homing and cellular traffic in lymph nodes. Nature Reviews Immunology. ISSN 1474-1741 (online).

25. Brown P. Lymphatic system:unlocking the drains. Nature. 2005;436:456-458.

26. Sherman AI, Pogossian TM. Lymph-node concentration of radioactive colloidal gold following interstitial injection. Cancer.1953;6(6)

27. Bergqvist L, Strand SE, Hafström L, Jönsson PE. Lymphoscintigraphy in patients with malignant melanoma: a quantitative and qualitative evaluation of its usefulness. Eur J Nucl Med. 1984;9(3):129-135.

28. Sullivan DC, Croker BP Jr, Harris CC, Deery P, Seigler HF. Lymphoscintigraphy in malignant melanoma: 99mTc antimony sulfur colloid. AJR Am J Roentgenol. 1981;137(4):847-851.

29. Bergqvist L, Strand SE. Autocorrelation spectroscopy for particle sizing and stability tests of radiolabelled colloids. Eur J Nucl Med. 1989;15(10):641-645.

30. Fokin AA, Robicsek F, Masters TN. Transport of viral-size particulate matter after intravenous versus intralymphatic entry. Microcirculation. 2000;7(5):357-365.

31. Giammarile F, Alazraki N, Aarsvold JN, Audisio RA, Glass E, Grant SF, Kunikowska J, Leidenius M, Moncayo VM, Uren RF, Oyen WJ, Valdés Olmos RA, Vidal Sicart S. The EANM and SNMMI practice guideline for lymphoscintigraphy and sentinel node localization in breast cancer. Eur J Nucl Med Mol Imaging. 2013;40(12):1932-1947.

32. Baker JL, Pu M, Tokin CA, Hoh CK, Vera DR, Messer K, Wallace AM. Comparison of [(99m)Tc]tilmanocept and filtered [(99m)Tc]sulfur colloid for identification of SLNs in breast cancer patients. Ann Surg Oncol. 2015 Jan;22(1):40-45.

33. Li N, Wang X, Lin B, Liu C, Xu X, Zhang Y, Zhai S, Ou Yang, Li J, Yang Z. Clinical Evaluation of 99mTc-Rituximab for Sentinel Lymph Node Mapping in Breast Cancer Patients. J Nucl Med. 2016;57(8):1214-1220.

34. Fang M, Chen M, Liu L, Li Y. Applications of Quantum Dots in Cancer Detection and Diagnosis: A Review. J Biomed Nanotechnol. 2017;13(1):1-16.

35. Radenkovic D, Kobayashi H, Remsey-Semmelweis E, Seifalian AM. Quantum dot nanoparticle for optimization of breast cancer diagnostics and therapy in a clinical setting. 2016;12(6):1581-1592.

36. Park J, Cho W, Park HJ, Cha KH, Ha DC, Choi YW, Lee HY, Cho SH, Hwang SJ. Biodistribution of newly synthesized PHEA-based polymer-coated SPION in Sprague Dawley rats as magnetic resonance contrast agent. Int J Nanomedicine. 2013;8:4077-4089.

37. Yu MK, Park J, Jeong YY, Moon WK, Jon S. Integrin-targeting thermally cross-linked superparamagnetic iron oxide nanoparticles for combined cancer imaging and drug delivery. Nanotechnology. 2010;21(41):415102.

38. Williams DB, Carter CB. Transmission electron microscopy. Springer; 2009. The transmission electron microscope; pp. 3–22.

39. Bootz A, Vogel V, Schubert D, Kreuter J. Comparison of scanning electron microscopy, dynamic light scattering and analytical ultracentrifugation for the sizing of poly(butyl cyanoacrylate) nanoparticles. Eur J Pharm Biopharm. 2004;57:369–375.

40. Johal M. Understanding Nanomaterials. 2011;ISBN 9781420073102.

41. Hall JB, Dobrovolskaia MA, Patri AK, McNeil SE. Characterization of nanoparticles for therapeutics. Nanomedicine. 2007;2:789–803.

42. Brar SK, Verma M. Measurement of nanoparticles by light-scattering techniques. TrAC Trends Anal Chem. 2011;30:4–17.

43. Di Marco M, Sadun C, Port M, Guilbert I, Couvreur P, Dubernet C. Int J Nanomedicine. 2007; 2(4):609-622.

44. [El-Gholabzouri O, Cabererizo-Vilchez MA, Hidalgo-Alvarez. Colloids and surfaces A: Physicochemical and engineering aspects.2006; 291(1-3):30-37.

45. Xu R. Progress in nanoparticles characterization:sizing and zeta potential measurement. Particuology. 2008;6(2):112-115.

46. Phelps M, Sorensen J. Physics in nuclear medicine.Elsevier, 4th Ed., ISBN: 978-1-4160-5198-5.

47. Sampath L, Wang W, Sevick-Muraca EM. Near infrared fluorescent optical imaging for nodal staging. J Biomed Opt. 2008 Jul-Aug;13(4):041312.

48. Sevick-Muraca EM. New horizons for imaging lymphatic function. Ann N Y Acad Sci. 2008;1131:13-36.

49. Unno N, Nishiyama M, Suzuki M, Yamamoto N, Inuzuka K, Sagara D, Tanaka H, Konno H. Quantitative lymph imaging for assessment of lymph function using indocyanine green fluorescence lymphography. Eur J Vasc Endovasc Surg. 2008 Aug;36(2):230-236.

50. Handgraaf HJ, Boogerd LS, Verbeek FP, Tummers QR, Hardwick JC, Baeten CI, Frangioni JV, van de Velde CJ, Vahrmeijer AL Intraoperative fluorescence imaging to localize tumors and sentinel lymph nodes in rectal cancer. Minim Invasive Ther Allied Technol. 2016;25(1):48-53.

51. Schaafsma BE, Verbeek FP, Rietbergen DD, van der Hiel B, van der Vorst JR, Liefers GJ, Frangioni JV, van de Velde CJ, van Leeuwen FW, Vahrmeijer AL. Clinical trial of combined radio- and fluorescence-guided sentinel lymph node biopsy in breast cancer. Br J Surg. 2013 Jul;100(8):1037-1044.

52. Xu Y, Liu H, Chang E, Jiang H, Cheng Z. Cerenkov Luminescence Imaging (CLI) for cancer therapy monitoring. J Vis Exp. 2012;(69):e4341.

53. Liu H, Carpenter CM, Jiang H, Pratx G, Sun C, Buchin MP, Gambhir SS, Xing L, Cheng Z. Intraoperative imaging of tumors using Cerenkov luminescence endoscopy: a feasibility experimental study. J Nucl Med. 2012;53(10):1579-84.

54. Das S, Thorek DL, Grimm J. Cerenkov imaging. Adv Cancer Res. 2014;124:213-234.

55. Thorek DLj, Robertson R, Bacchus WA, Hahn J, Rothberg J, Beattie BJ, Grimm J. Cerenkov imaging - a new modality for molecular imaging. Am J Nucl Med Mol Imaging. 2012;2(2):163-173.

56. Kjellman P, Fredriksson S, Zandt R, Strand S-E. Optimizing retention of multimodal imaging nanostructures in sentinel lymph nodes by nanoscale size tailoring. Nanomedicine: nanotechnology biology and medicine. 2014;10(5):1089-1095.

57. Li SD, Huang. Pharmacokinetics and biodistribution of nanoparticles. Mol Pharm. 2008;5(4):496-504.

58. Siram K, Marslin G, Raghavan CV, Balakumar K, Rahman H, Franklin G. A brief perspective on the diverging theories of lymphatic targeting with colloids. 2016;147:274-280.

59. Karthik S, Raghavan CV, Marslin G, Rahman H, Selvaraj D, Balakumar K, Franklin G. Quillaja saponin: A prospective emulsifier for the preparation of solid lipid nanoparticles. Colloids Surf B Biointerfaces. 2016;147:274-280.

60. Bergqvist L, Sundberg R, Rydén S, Strand SE. The "critical colloid dose" in studies of reticuloendothelial function. J Nucl Med. 1987;28(9):1424-1429.

61. Mease RC, Lambert C. Newer methods of labeling diagnostic agents with Tc-99m. Semin Nucl Med. 2001;31(4):278-285.

62. Torres Martin de Rosales R, Tavaré R, Glaria A, Varma G, Protti A, Blower PJ. (^{99m})Tc-bisphosphonate-iron oxide nanoparticle conjugates for dual-modality biomedical imaging. Bioconjug Chem. 2011;22(3):455-465.

63. Lamb J, Holland JP. Advanced Methods for Radiolabeling Multimodality Nanomedicines for SPECT/MRI and PET/MRI. J Nucl Med. 2018;59(3):382-389.

64. Velikyan I. Continued rapid growth in (68) Ga applications: update 2013 to June 2014. J Labelled Comp Radiopharm. 2015;58(3):99-121.

64 Ferreira CL, Japp D, Mandel D, Gill R, Boros E, Wong M, Jurek P, Kiefer GE. 68Ga Small Petptide imaging:comparison of NOTA and PCTA. Bioconjugate Chem., 2012;*23* (11): 2239–2246.

65 Schiller E, Bergmann R, Wunderlich G, Andreeff M, Jacob A and Pietzsch. Ga-68- and Cu-64-Labeled NOTA-Albumin Conjugates for PET Sentinel Lymph Node Imaging. ISNRN Molecular Imaging. 2013; 386976.

66 Hofman MS, Hicks RJ, Maurer T, Eiber M. Prostate-specific Membrane Antigen PET: Clinical Utility in Prostate Cancer, Normal Patterns, Pearls, and Pitfalls. Radiographics. 2018 Jan-Feb;38(1):200-217.

67 Burke BP, Baghdadi N, Kownacka A et al. Chelator free gallium-68 radiolabellimg of silica coated iron oxide nanorode via surface interactions. Nanoscale.2015;7:14889.

68 Holland JP, Ferdani R, Anderson CJ, Lewis JS. Copper-64 Radiopharmaceuticals for Oncologic Imaging. J Nucl Med. 2009;50(4):625-34.

69 Anderson CJ, Ferdani R. Copper-64 radiopharmaceuticals for PET imaging of cancer: advances in preclinical and clinical research. Cancer Biother Radiopharm. 2009 Aug;24(4):379-93.

70 Torres RMR, Tavaré R, Rowena LP, Jauregui-Osoro M, Protti A, Glaria A, Varma G, Szanda I, Blower JP. Synthesis of 64CuII Bis(dithiocarbamatebisphosphonate) and Its Conjugation with Superparamagnetic Iron Oxide Nanoparticles: In Vivo Evaluation as Dual-Modality PET–MRI Agent. Angew Chem Int Ed Engl. 2011; 50(24):5509–5513.

71 Glaus C, Rossin R, Welch MJ, Bao G. In vivo evaluation of ^{64}Cu-labeled Magnetic Nanoparticles as a Dual-Modality PET/MR Imaging Agent. Bioconjug Chem. 2010;21(4):715–722.

72 Min Zhou, Rui Zhang, Miao Huang, Wei Lu, Shaoli Song, Marites P. Melancon, Mei Tian, Dong Liang, Chun Li. A Chelator-Free Multifunctional [64Cu]-CuS Nanoparticle Platform for Simultaneous Micro-PET/CT Imaging and Photothermal Ablation Therapy. J Am Chem Soc. 2010;132(43):15351–15358.

73 Petersen AL1, Henriksen JR, Binderup T, Elema DR, Rasmussen PH, Hag AM, Kjær A, Andresen TL In vivo evaluation of PEGylated ^{64}Cu-liposomes with theranostic and radiotherapeutic potential using micro PET/CT. Eur J Nucl Med Mol Imaging. 2016;43(5):941-952.

74 Tilney NL. Patterns of lymphatic drainage in the adult laboratory rat. J Anat. 1971;109(3):369–383.

75 Leung K. Gadolinium-G6 dendrimer-Cy5.5. Biotechnology Information (US); 2004-2013.

76 Zhu T, Ma X, Chen R, Ge Z, Xu J, Shen X, Jia L, Zhou T, Luo Y, Ma T. Using fluorescently-labeled magnetic nanocomposites as a dual contrast agent for optical and magnetic resonance imaging. Biomater Sci. 2017;5(6):1090-1100.

77 Pluim JP, Maintz JB, Viergever MA. Image registration by maximization of combined mutual information and gradient information. IEEE Trans Med Imaging. 2000;19(8):809-14.

Printed by Media-Tryck, Lund 2018 NORDIC SWAN ECOLABEL 3041 0903

Multimodality Imaging
PET / CT / SPECT / MRI /Optical / Cherenkov Luminescence
A noninvasive technique based on high sensitivity and high-resolution images are warranted for in vivo diagnostics, therapy planning and follow up. In order to meet this, we combine the strength of several imaging modalities by developing a single contrast agent for combined SPECT or PET /Magnetic Resonance /Optical/ Ultrasound and Photoacoustic imaging.

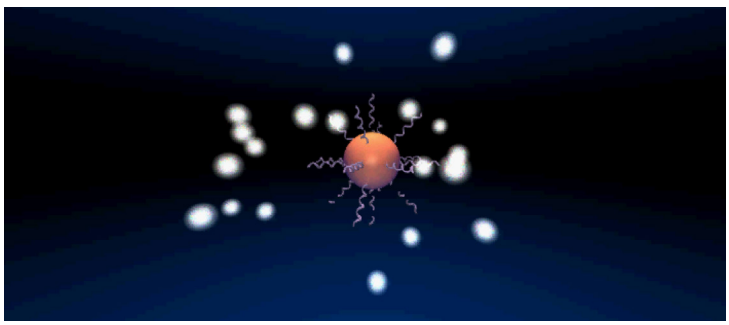

LUND UNIVERSITY

FACULTY OF SCIENCE

Lund University
Faculty of science
Department of Medical Radiation Physics
ISBN 978-91-7753-685-7